The promotion effect of nitrous acid on aerosol formation in wintertime Beijing: possible contribution of traffic-related emission

Yongchun Liu[1*], Yusheng Zhang[1], Chaofan Lian[2,6], Chao Yan[3], Zeming Feng[1], Feixue Zheng[1], Xiaolong Fan[1], Yan Chen[2,6], Weigang Wang[2,6*], Biwu Chu[3,4], Yonghong Wang[3], Jing Cai[3], Wei Du[3], Kaspar R. Daellenbach[3], Juha Kangasluoma[1,3], Federico Bianchi[1,3], Joni Kujansuu[1,3], Tuukka Petäjä[3], Xuefei Wang[6], Bo Hu[5], Yuesi Wang[5], Maofa Ge[2], Hong He[4] and Markku Kulmala[1,3*]

1. Aerosol and Haze Laboratory, Advanced Innovation Center for Soft Matter Science and Engineering, Beijing University of Chemical Technology, Beijing, 100029, China

2. State Key Laboratory for Structural Chemistry of Unstable and Stable Species, Beijing National Laboratory for Molecular Sciences, Institute of Chemistry, Chinese Academy of Sciences, Beijing 100190, China

3. Institute for Atmospheric and Earth System Research/Physics, Faculty of Science, University of Helsinki, P.O. Box 64, FI-00014, Finland

4. State Key Joint Laboratory of Environment Simulation and Pollution Control, Research Center for Eco-Environmental Sciences, Chinese Academy of Sciences, Beijing, 100085, China

5. State Key Laboratory of Atmospheric Boundary Layer Physics and Atmospheric Chemistry, Institute of Atmospheric Physics, Chinese Academy of Sciences, Beijing, 100029, China

6. University of Chinese Academy of Sciences, Beijing 100049, PR China

Correspondence to: liuyc@buct.edu.cn, wangwg@iccas.ac.cn or markku.kulmala@helsinki.fi

Abstract

Secondary aerosol is a major component of $PM_{2.5}$, yet its formation mechanism in the ambient atmosphere is still an open question. Based on field measurements in downtown Beijing, we show that the photolysis of nitrous acid (HONO) might promote the formation of organic and nitrate aerosol in wintertime Beijing as evidenced by the growth of the mass concentration of organic and nitrate aerosols linearly increasing as a function of consumed HONO from early morning to noon. The increased nitrate also leads to the formation of particulate matter ammonium by enhancing the neutralization of nitrate and sulfate by ammonia. We further illustrate that over 50 % of the ambient HONO during pollution events in wintertime Beijing might be related to traffic-related emission including direct emission and formation via the reaction between OH and vehicle-emitted NO. Overall, our results indicate that the traffic-related HONO might play an important role in the oxidative capacity and in turn, contribute to the haze formation in winter Beijing. Mitigation of HONO and NO_x emission from the vehicles might be an effective way to reduce secondary aerosol mass formation and severe haze events in wintertime Beijing.

1. Introduction

China is one of the countries suffering from severe pollution of fine particulate matter with diameter less than or equal to 2.5 μm ($PM_{2.5}$) (Lelieveld et al., 2015). Although the regional air quality has been continuously improving since the central government of China issued the Clean Air Act in 2013 (Vu et al., 2019), $PM_{2.5}$ concentration is still significantly higher than that in developed countries (Fu et al., 2014;An et al., 2019). Nowadays, a consensus has been reached that haze events are driven by local emissions (An et al., 2019), regional transport (Zheng et al., 2015b) and secondary formation (Huang et al., 2014;He et al., 2018) of pollutants under unfavorable meteorological conditions (stagnant atmosphere and high relative humidity) (Zhu et al., 2018;Liu et al., 2017c). A feedback loop between meteorological parameters and haze formation also plays an important role in the evolution of haze events (Zhang et al., 2018b).

Secondary aerosol can contribute ~70 % to the aerosol mass concentration on polluted days (Huang et al., 2014). Several reaction pathways have been proposed, such as sulfate formation via heterogeneous oxidation of SO_2 promoted by H_2O_2 and/or NO_2 on mineral dust (Huang et al., 2015;He et al., 2014), aqueous oxidation of SO_2 promoted by NO_2 in the presence or absence of NH_3 in particle-bound water film (He et al., 2014;Wang et al., 2016), catalytic conversion of SO_2 to sulfate by black carbon (Zhang et al., 2020), nitrate formation via efficient hydrolysis of N_2O_5 on aerosol surfaces (Wang et al., 2017c;Wang et al., 2019;Kulmala, 2018;Li et al., 2017), and the haze formation initiated by new particle formation and growth (Guo et al., 2014;Guo et al., 2020). During the past years, strict control of coal combustion has successfully reduced

64 the SO_2 concentration, resulting in a reduction of sulfate (SO_4^{2-}) component in $PM_{2.5}$;
65 in stark contrast, the contributions from organic and nitrate become increasingly more
66 significant in China (Lang et al., 2017).

67 The formation of secondary organic aerosol (SOA) starts from the gas-phase
68 oxidation of volatile organic compounds (VOCs) leading to various low-volatility and
69 semi-volatile products (Bianchi et al., 2019), followed by partitioning into the particle
70 phase (Hallquist et al., 2009). Similarly, the formation of nitrate aerosol in the daytime
71 is largely due to the partitioning of gaseous nitric acid, which is formed via the oxidation
72 of NO_2 by OH (Seinfeld and Pandis, 2006;Wang et al., 2019). It is traditionally believed
73 that the wintertime atmospheric oxidation capacity is weak due to the weak solar
74 radiation, which limits the formation of SOA and nitrate (Sun et al., 2013). However, it
75 is very recently shown that the peak OH concentration on polluted days in winter
76 Beijing varies from 2×10^6 to 6×10^6 molecules cm^{-3}, which is 6-10 times higher than
77 what is predicted by the global model (Tan et al., 2018). This discrepancy can be largely
78 reduced after accounting for other OH production processes in model simulations,
79 which shows that the photolysis of nitrous acid (HONO) dominates the initiation of
80 HO_x (OH and HO_2) and RO_x (RO and RO_2) radical chain in wintertime Beijing (Tan et
81 al., 2018), and some other cities (Ren et al., 2006;Stutz et al., 2013).

82 More recently, modeling studies have suggested that nitrous acid (HONO) could
83 enhance secondary aerosols formation in Beijing-Tianjin-Hebei (BTH) region (Zhang
84 et al., 2019b), Pearl-River-Delta (PRD) region of China (Zhang et al., 2019a;Xing et
85 al., 2019) and Houston (Czader et al., 2015). These results imply that the role of HONO

in haze chemistry might be crucial in wintertime Beijing, while the direct evidence from observation has not been reported, yet. On the other hand, the HONO budget has been investigated via modeling studies (Liu et al., 2019c;Zhang et al., 2019b) and photostationary state calculations (Wang et al., 2017b;Li et al., 2018;Huang et al., 2017b;Lee et al., 2016;Oswald et al., 2015) at different locations. At the present time, the study of the HONO budget is still far from closed, which would require a significant effort on both the accurate measurement of HONO and the determination of related kinetic parameters for its production pathways (Liu et al., 2019c). For example, photo-enhanced conversion of NO_2 (Su et al., 2008) and photolysis of particulate nitrate were found to be two major mechanisms with large potential of HONO formation during noontime, but the associated uncertainty may reduce their importance (Liu et al., 2019c). Some other researches proposed that heterogeneous reactions on ground/aerosol surfaces were important during nighttime (Wang et al., 2017b;Zhang et al., 2019b) and daytime in Beijing-Tianjin-Hebei (BTH) (Zhang et al., 2019b). But the heterogeneous reaction was unimportant in Ji'an compared with the unknown sources and the homogeneous reaction between NO and OH (Li et al., 2018). In addition, the traffic emission was proposed to be an important HONO source during nighttime but not significant during daytime in BTH (Zhang et al., 2019b). However, it was proposed that direct emission of HONO from vehicles should contribute about 51.1 % (Meng et al., 2019) and 52 % of nighttime HONO in Beijing (Zhang et al., 2018a). These results mean that more studies is still required on the HONO budget. In particular, it is meaningful to analyze the HONO budget in polluted events for understanding the

possible influence of HONO sources on secondary pollutants formation.

In this work, we carried out comprehensive measurements at a newly constructed observation station (Aerosol and Haze Laboratory, Beijing University of Chemical Technology, AHL/BUCT Station) located in the western campus of Beijing University of Chemical Technology in downtown Beijing. We show observational evidence that HONO might have a prominent promotion effect on the secondary aerosol mass formation in winter. Traffic-related emission seems to be a vital contributor to ambient HONO during the pollution events in winter in Beijing.

2. Materials and methods

2.1 Field measurements. Field measurements were performed at AHL/BUCT Station (Lat. 39º56′31″ and Lon. 116º17′52″) from February 1 to June 30, 2018. The observation station is on a rooftop of the main building, which is 550 m from the 3rd ring road in the East, 130 m from the Zizhuyuan road in the North and 565 m from the Nandianchang road in the West (Figure S1). The station is surrounded by both traffic and residential emissions, thus, is a typical urban observation site.

Ambient air was sampled from the roof of five floors (~18 m above the surface). A $PM_{2.5}$ inlet (URG) was used to cut off the particles with diameter larger than 2.5 μm before going to a Nafion dryer (MD-700-24, Perma Pure). Then a Time-of-Flight Aerosol Chemical Speciation Monitor equipped a $PM_{2.5}$ aerodynamic lens (ToF-ACSM, Aerodyne) and an Aethalometer (AE33, Magee Scientific) were connected to the manifold of aerosol sampling tube. The Reynolds number in the aerosol sampling tube was 800 with the total flow rate of 16.7 lpm and the residence time of 6.5 s. The details

about ToF-ACSM measurement was described in the Supplement information. Ambient air was drawn from the roof using a Teflon sampling tube (BMET-S, Beijing Saak-Mar Environmental Instrument Ltd.) with the residence time <10 s for gas-phase pollutants measurements. Trace gases including NOx, SO_2, CO and O_3 were measured with the corresponding analyzer (Thermo Scientific, 42i, 43i, 48i and 49i). Volatile organic compounds (VOCs) was measured using an online Single Photon Ionization Time-of-flight Mass Spectrometer (SPI-ToF-MS 3000R, Hexin Mass Spectrometry) with unit mass resolution (UMR). The principle and the configuration of the instrument has been described in detail elsewhere (Gao et al., 2013) and the Supplement information. HONO concentration was measured using a home-made Long Path Absorption Photometer (LOPAP) (Tong et al., 2016). The details are described in the Supplement information. Particle size and number concentration from 1 nm to 10 μm were measured with a Scanning Mobility Particle Sizer (SMPS 3936, TSI), a particle size magnifier (PSM, Airmodus) and a Neutral Cluster and Air Ion Spectrometer (NIAS, Airel Ltd.). Meteorological parameters including temperature, pressure, relative humidity (RH), wind speed and direction were measured using a weather station (AWS310, Vaisala). Visibility and planetary boundary layer (PBL) height were measured using a visibility sensor (PWD22, Vaisala) and a ceilometer (CL51, Vaisala), respectively

2.2 HONO budget calculation. Several sources of ambient HONO have been identified, such as emission from soil (E_{soil}) (Oswald et al., 2015;Meusel et al., 2018) and vehicle exhaust ($E_{vehicle}$) (Trinh et al., 2017), production through homogeneous

reaction between NO and OH ($P_{NO\text{-}OH}$) in the atmosphere, photolysis of nitrate ($P_{nitrate}$) (Bao et al., 2018), nitrous acid (P_{HNO3}) and nitrophenenol ($P_{nitrophenol}$) (Sangwan and Zhu, 2018), heterogeneous reaction of NO_2 on aerosol surface ($P_{aerosol}$) (Liu et al., 2015) and ground surface (P_{ground}) (Liu et al., 2019c;Li et al., 2018;Wang et al., 2017b). However, the photolysis of HNO_3 and nitrophenol were excluded in this work because they were believed as minor sources (Lee et al., 2016) and their concentrations were unavailable during our observation. The removal pathways of HONO including photolysis ($L_{photolysis}$), the homogeneous reaction with OH radical ($L_{HONO\text{-}OH}$) and dry deposition ($L_{deposition}$) (Liu et al., 2019c) were considered.

The HONO budget could be calculated by,

$$\frac{dc_{HONO}}{dt} = E_{HONO} + P_{HONO} - L_{HONO} + T_{vertical} + T_{horizontal} \quad (1)$$

where $\frac{dc_{HONO}}{dt}$ is the observed change rate of HONO mixing ratios (ppbv h^{-1}); E_{HONO} represents the emission rate of HONO from different sources (ppbv h^{-1}); P_{HONO} is the in-*situ* production rate of HONO in the troposphere (ppbv h^{-1}); L_{HONO} is the loss rate of HONO (ppbv h^{-1}) (Li et al., 2018); $T_{vertical}$ and $T_{horizontal}$ are the vertical and horizontal transport (Soergel et al., 2011), which can mimic source or sink terms depending on the HONO mixing ratios of the advected air relative to that of the measurement site and height (Soergel et al., 2011).

The emission rate (E_{HONO}, ppbv h^{-1}) was calculated based on the emission flux (F_{HONO}=EI_{HONO}/A, g m^{-2} s^{-1}) and PBL height (H, m) according to the following equation,

$$E_{HONO} = \frac{a \cdot F_{HONO}}{H} \quad (2)$$

where, EI_{HONO}, is the emission inventory of HONO (g s^{-1}), A is the core urban area of

Beijing (m^2, with 20 km of diameter), α is the conversion factor ($\alpha = \frac{1\times10^9\cdot3600\cdot R\cdot T}{M\cdot P} = \frac{2.99\times10^{13}\cdot T}{M\cdot P}$), M is the molecular weight (g mol^{-1}), T is the temperature (K) and P is the atmospheric pressure (Pa).

The production rates of HONO (P_{HONO}, ppbv h^{-1}) in the troposphere was calculated by,

$$P_{HONO} = 3600 \cdot k_1 \cdot c_{precursor} \quad (3)$$

where, k_1 is the quasi first-order reaction rate constant (s^{-1}), $c_{precursor}$ is the concentration of precursor (ppbv). For homogeneous reaction between NO and OH,

$$k_1 = k_2 \cdot c_{OH} \quad (4)$$

where, k_2 is the second-order reaction rate constant (7.2×10^{-12} cm^3 $molecule^{-1}$ s^{-1}) (Li et al., 2012), c_{OH} is the OH concentration (molecules cm^{-3}). For heterogeneous reaction,

$$k_1 = \frac{\gamma\cdot A_s\cdot\omega}{4} \cdot Y_{HONO} \quad (5)$$

where, A_s is the surface area concentration of the reactive surface (m^2 m^{-3}), ω is the molecular mean speed (m s^{-1}), γ is the uptake coefficient of the precursor, Y_{HONO} is the yield of HONO. For ground surface, the surface area concentration is

$$A_s = \frac{\delta}{H} \quad (6)$$

where δ is the surface roughness, which is calculated according to the mean project area, perimeter and height of the buildings in Beijing.

$$\delta = \frac{f_{building}*(A_{projected}+h*P_{building})}{A_{projected}} + f_{blank} \quad (7)$$

where $f_{building}$ (0.31) and f_{blank} (0.69) are the fraction of the projected area ($A_{projected}$) of buildings and blank space, respectively; $P_{building}$ and h are the perimeter and the height of the building, respectively. The $f_{building}$ and $P_{building}$ are measured from ~1000 buildings

196 randomly selected on the Google Map using ImageJ software. The mean height (44.5
197 m) of the building in Beijing is linearly extrapolated from the literature data based on
198 remote measurement using Light Detection and Ranging (LiDAR) sensor from 2004 to
199 2008 (Cheng et al., 2011). The δ in Beijing is calculated to be 3.85, which is slightly
200 higher than the value (2.2) used by Li et al. (2018).

201 As for photolysis reaction, the first-order reaction rate was

202 $$k_1 = J \quad (8)$$

203 where, J is the photolysis rate to produce HONO (s^{-1}).

204 The loss rates of HONO by photolysis ($L_{photolysis}$), homogeneous reaction with
205 OH radicals ($L_{HONO\text{-}OH}$) and dry deposition ($L_{deposition}$) (Liu et al., 2019c) were calculated
206 according to the following equations.

207 $$L_{photolysis} = 3600 \cdot J_{HONO} \cdot c_{HONO} \quad (9)$$

208 $$L_{HONO-OH} = 3600 \cdot k_{HONO-OH} \cdot c_{OH} \cdot c_{HONO} \quad (10)$$

209 $$L_{deposition} = \frac{3600 \cdot v_d \cdot c_{HONO}}{H} \quad (11)$$

210 where, J_{HONO} is the photolysis rate of HONO (s^{-1}), $k_{HONO\text{-}OH}$ is the second-order reaction
211 rate constant between HONO and OH (6×10^{-12} cm^3 $molecule^{-1}$ s^{-1}) (Atkinson et al.,
212 2004), and v_d is the dry deposition rate of HONO (0.001 m s^{-1}) (Han et al., 2017).

213 Vertical transport by advection ($T_{vertical}$), which is an important sink of HONO in
214 the night (Gall et al., 2016;Meng et al., 2019), can be calculated according to equation
215 (12).

216 $$T_{vertical} = -K_h(z,t)\frac{\partial c(z,t)}{\partial z}\frac{1}{h} \quad (12)$$

217 where K_h(z,t) is the eddy diffusivity of heat (m^2 s^{-1}) at height z (m) and time t, h is the

height of the second layer (18 m in this study) (Gall et al., 2016). On the other hand, both the vertical and horizontal transport can be estimate according to Eq. (13),

$$T_{vertical} = k_{dilution}(c_{HONO} - c_{HONO,background}) \quad (13)$$

where $k_{dilution}$ is a dilution rate (0.23 h^{-1}, including both vertical and horizontal transport) (Dillon et al., 2002), c_{HONO} and $c_{HONO,background}$ is the HONO concentration at the observation site and background site, respectively (Dillon et al., 2002).

In addition, even though all the current known sources had been considered in models, the modelled daytime HONO concentrations were still lower than the observed concentration (Tang et al., 2015;Michoud et al., 2014). Therefore, the HONO concentration could be described in equation (14).

$$\frac{dc_{HONO}}{dt} = E_{soil} + E_{vehicle} + P_{NO-OH} + P_{nitrate} + P_{aerosol} + P_{ground} + P_{unknown} - L_{photolysis} - L_{HONO-OH} - L_{deposition} + T_{vertical} + L_{horizontal} \quad (14)$$

3. Results and discussion

3.1 Overview of the air pollution. The mass concentration of non-refractory $PM_{2.5}$ (NR-$PM_{2.5}$) and HONO along with metrological parameters are shown in Fig. 1. The time series of other pollutants (SO_2, CO, O_3, benzene, toluene and black carbon) are shown in Fig. S2 in the Supplement information.

Similar to previous measurements (Guo et al., 2014;Wang et al., 2016), the air pollution events showed a periodic cycle of 3-5 days during the observation, as indicated by the concentration of NR-$PM_{2.5}$ (Fig. 1A), gaseous pollutants and the visibility. During the observation period, 20-60% of hourly $PM_{2.5}$ concentration was higher than 75 μg m^{-3} (the criterion for pollution according to the national air quality

standards) in each month (Fig. S3A). Both the frequency of severe polluted episodes and the mean mass concentration of $PM_{2.5}$ and NR-$PM_{2.5}$ were obviously higher in March than that in the rest months (Fig. 1 and S3). This can be explained by both the intensive emission during the heating season as evidenced by the high concentration of primary pollutants including CO, SO_2 and BC (Table S1) and the stagnant meteorological conditions supported by the low wind speed (<2 m s^{-1}) and planetary boundary layer (PBL) height in March (Fig. S4A).

OA and nitrate dominated the NR-$PM_{2.5}$, while their relative contribution varied significantly during the observation (Fig. 1B and Table S1). This is similar to the previously reported NR-$PM_{1.0}$ composition (Sun et al., 2015). The monthly mean fraction of OA varied from 45.9±10.2 % to 52.6±18.7 %, which was accompanied by a slight increase of sulfate from 16.0±9.1 % to 18.2±8.0 % (Fig. S4D). At the same time, the monthly mean fraction of nitrate and chloride decreased from 26.7±8.8 % to 16.7±12.8 % and from 7.7±6.1 % to 0.3±0.2 %, respectively. Ammonium showed a peak value (14.2±2.8 %) in March, then slightly decreased to 12.2±5.2 %. The intensive emission of chloride from coal combustion during heating season (Cho et al., 2008) and firework burning (Zhang et al., 2017), which was transported from Tangshan during Chinese New Year (Fig. S5A and B), led to high fraction of chloride in February and March. The decrease in nitrate and ammonium fractions from February to June should be related to the increase in temperature (Fig. S2) which was in favor of NH_4NO_3 decomposition (Wang et al., 2015). Besides the reduction of the contribution from other components, secondary formation due to increased UV light (Fig. S4C) might also

favor the increased OA fraction (Huang et al., 2014). This means that chemical transformation in March should still be vigorous although the UV light intensity in March is lower than in summer (Fig. S4C). It also implies other factors may compensate the weak UV light intensity in March.

HONO, which has been recognized as the important precursor of primary OH radical (Ren et al., 2006;Alicke et al., 2003), ranged from 0.05 to 10.32 ppbv from February 1 to June 30, 2018 (Fig. 1C) with the mean value of 1.26±1.06 ppbv. In winter (February and March), HONO concentration was 1.15±1.10 ppbv and comparable to the previous results (1.05±0.89 ppbv) measured in the winter of Beijing (Wang et al., 2017b;Hou et al., 2016), while it was slightly lower than that from April to June (1.35±1.11 ppbv) in this work and those measured in the summer of Shanghai (2.31 ppbv, in May) (Cui et al., 2018) and Guangzhou (2.8 ppbv, in July) (Qin et al., 2009). The mean HONO concentration in March (1.53±1.25 ppbv) was higher than that in February and April (Fig. S3D), while was slightly higher or close to that in May and June. Chamber studies have found that HONO is responsible for the initiation of photosmog reactions (Rohrer et al., 2005). It is reasonable to postulate that HONO probably play an important role in the secondary chemistry of particle formation in March.

3.2 Possible promotion effect of HONO photolysis on aerosol formation in winter.

Oxidation of precursors by OH radicals is the main mechanism regarding to secondary aerosol formation in the troposphere. After partially ruling out the possible influence of PBL variation by normalizing the concentrations of all pollutants to CO (Cheng et al.,

2016) or BC (Liggio et al., 2016), we found all secondary species including sulfate, nitrate and ammonium show obvious daytime peaks from 7:00 am to 6:00 pm (Figure S5C) (Cheng et al., 2016). The similar trends were observed after the concentrations of pollutants were normalized to BC (not shown). This suggests they might connect with photochemistry.

Photolysis of H_2O_2, HCHO, O_3 and HONO, and the reaction between NO and HO_2 are known as sources of OH radical in the atmosphere (Alicke et al., 2003;Volkamer et al., 2010;Tan et al., 2018;Tang et al., 2015). In this work, the concentration of H_2O_2, HCHO and HO_2 are unavailable. Thus, their contributions to OH production were not discussed here. However, it has been well recognized that the photolysis of HONO is the dominant source of OH in the dawn and dusk period (Holland et al., 2003), even contributes up to 60% of daytime OH source in winter (Spataro et al., 2013;Rohrer et al., 2005). In addition, it has been confirmed that HONO dominates the primary OH source at various locations (Tan et al., 2018;Liu et al., 2019c;Tan et al., 2017;Aumont et al., 2003). Therefore, it is meaningful to discuss the possible contribution of HONO to secondary aerosol formation through OH production. We simply compared the OH production via photolysis of HONO ($P_{OH\text{-}HONO}=J_{HONO}\times c_{HONO}$) and O1D production rate from O_3 ($P_{O1D}=J_{O1D}\times c_{O3}$) in Fig. 2 when the $PM_{2.5}$ concentration was larger than 50 μg m^{-3} and the RH was less than 90 % to understand the chemistry in pollution events. Under these conditions, local chemistry should be more important as 75 % of the wind speed was less than 1.0 m s^{-1} (Fig. S6). The details about the J_{HONO} and J_{O1D} calculation were shown in the Supplement information and their time series were shown in Fig. S7.

On polluted days in winter, the daytime $P_{OH\text{-}HONO}$ was always significantly higher than the $P_{OH\text{-}O3}$ in winter and the maximal $P_{OH\text{-}HONO}$ and P_{O1D} were 1.73±0.86 × 10^7 molecules cm^{-3} s^{-1} (2.43±1.21 ppb h^{-1}) and 1.03±1.06 × 10^7 molecules cm^{-3} s^{-1} (1.45±1.49 ppb h^{-1}), respectively (Fig. 2A). Owing to the high HONO concentration accumulated throughout the night, the maximal $P_{OH\text{-}HONO}$ in winter was as about 2-6 times of that was observed in the wintertime of Colorado, USA (~0.59 ppb h^{-1}) (Kim et al., 2014), New York, USA (~0.40 ppb h^{-1}) (Kanaya et al., 2007) and Nanjing, China (0.90±0.27 ppb h^{-1}) (Liu et al., 2019b). In the period from April to June, the daily maxima of $P_{OH\text{-}HONO}$ and P_{O1D} were 2.48±1.42 ×10^7 molecules cm^{-3} s^{-1} (3.48±1.99 ppb h^{-1}) and 6.51±4.17 ×10^7 molecules cm^{-3} s^{-1} (9.15±5.86 ppb h^{-1}), respectively. Because the production of OH from photolysis of O_3 should be directly proportion to P_{O1D}, these results imply that the relative importance of the photolysis of HONO compared with that of O_3 for initiating the daytime HO_x and RO_x chemistry on polluted days should be more important in winter than that from April to June. This is consistent with the previous findings that HONO photolysis dominants the primary OH source in winter of BTH (Xing et al., 2019;Tan et al., 2018), Colorado and New York City (Ren et al., 2006;Kim et al., 2014), while photolysis of O_3 and HCHO related reactions usually dominated OH production in summer (Alicke et al., 2003).

Oxidation of trace gas pollutants, in particular VOCs, by OH is their main removal pathway in the troposphere (Atkinson and Arey, 2003), subsequently contribute to secondary aerosol formation (Kroll and Seinfeld, 2008). A very recent work has found that oxidation of VOCs from local traffic emission is still efficient even under pollution

conditions (Guo et al., 2020). This means high HONO concentration might promote SOA formation after sunrise because HONO is an important primary OH source in the early morning. To confirm this assumption, 12 episodes in winter were further analyzed (Fig. 1). The dataset under stagnant meteorological conditions as indicated by the low wind speed (< 1.0 m s^{-1}, Fig. S5D) was analyzed to decrease the contribution of transport to the observed HONO and OA. The 1st, 3rd and 5th episodes were clean days and the other 9 episodes were typical haze events with duration above 2 days. The features of these episodes were summarized in Table S2. Fig. 2C shows the CO-normalized daytime profiles of OA and HONO in the 7th and 12th episodes as two examples. In all the selected cases, HONO exhibited quick reduction due to the photolysis after sunrise, and simultaneously, OA concentration started to increase. This is similar to the evolution of the concentration of pollutants in a typical smog chamber experiment. We further show the formation of OA ($\Delta C_{OA}/C_{CO}$) as a function of the consumed HONO ($-\Delta C_{HONO}/C_{CO}$) in Fig. 2D. Except for the 4th episode that was highly affected by firework emission during the Spring Festival, $\Delta C_{OA}/C_{CO}$ showed a linear dependence on $-\Delta C_{HONO}/C_{CO}$ in winter (R=0.75). This kind of correlation could not be seen for the pollution events from April to June because the relative importance of HONO photolysis in primary OH production decreased as indicated by Fig. 2D. It should be noted that oxidation of biogenic alkenes by O_3 might also contribute to OA formation. However, anthropogenic VOCs instead of biogenic VOCs dominated the wintertime VOCs in Beijing (Liu et al., 2017a). Although vehicles can emit isoprene (Zou et al., 2019), the contribution of isoprene to the observed increase of OA

concentration should be unimportant due to the low concentration of isoprene in winter (Zou et al., 2019). Therefore, it is reasonable to conclude that the increase of OA concentration in daytime might be mainly resulted from oxidation of VOCs by OH.

Similar to OA, $\Delta C_{nitrate}/C_{CO}$ in winter also showed good linear correlation with $-\Delta C_{HONO}/C_{CO}$ (R=0.67, Fig. S5E), suggesting that the increase of particle-phase nitrate in the daytime should also be promoted by OH radical. Interestingly, $\Delta C_{ammonium}/CO$ also showed a good correlation with $-\Delta C_{HONO}/C_{CO}$ (R=0.61, Fig. S5E), although particle-phase ammonium should not be directly related to oxidation of NH_3 by OH. We explained the increased ammonium as the result of enhanced neutralization of sulfate and nitrate by NH_3 (Wang et al., 2018;Wen et al., 2018;Sun et al., 2018) because NH_4^+ was adequate to neutralize both sulfate and nitrate as shown in Fig.S8. This was consistent with the recent work which observed the important role of photochemical reactions in daytime nitrate formation, while hydrolysis of N_2O_5 mainly contributed to nighttime nitrate (Tian et al., 2019). Although a recent work has found that daytime hydrolysis of N_2O_5 on hygroscopic aerosols is also an important source of daytime nitrate in winter Beijing (Wang et al., 2017a), the linearly correlation between $\Delta C_{nitrate}/C_{CO}$ and $\Delta C_{HONO}/C_{CO}$ at least implies that the promotion effect of HONO on nitrate formation could not be excluded. On the other hand, the correlation between $\Delta C_{sulfate}/C_{CO}$ and $-\Delta C_{HONO}/C_{CO}$ was much weaker (R=0.26), suggesting a weak connection between particle-phase sulfate and gas-phase H_2SO_4. This was also consistent with the previous understanding that heterogeneous reactions of SO_2 were the dominant pathway for sulfate formation (Zheng et al., 2015a;He et al., 2018;Zhang

et al., 2020). Overall, this work qualitatively supported the recent modeling results that HONO might promote the aerosol production in winter (Zhang et al., 2019a;Zhang et al., 2019b;Xing et al., 2019;An et al., 2013) from the point of view of observation.

3.3 HONO budget in polluted events. To understand the possible sources of HONO in polluted events in winter, the HONO budget was calculated for the events when the $PM_{2.5}$ concentration was larger than 50 μg m^{-3} and the RH was less than 90 % according to the method described in Section 2.2.

Vehicle emission. The $E_{vehicle}$ was calculated in the light of Eq. (2) using the relative emission rate of HONO to NO_x and the emission inventory of NO_x from vehicles. Firstly, the ratio of HONO/NO_x was calculated according to the method reported by Xu et al. (Xu et al., 2015) and Li et al. (Li et al., 2018) from the fresh nighttime plumes which were strictly satisfy the following criteria: 1) NO_x > 45 ppb (highest 25% of NO_x data); 2) $\Delta NO/\Delta NO_x$ > 0.8, with good correlation between NO and NO_x (R > 0.9, P < 0.05); 3) Good correlation between HONO and NO_x (R^2>0.65, P < 0.05); and 4) Dataset from 5:00 am to 8:00 am. The mean emission ratio of HONO to NO_x was 1.8±0.5% based on 5 fresh vehicle exhaust plumes during our observation (Table S3). This value is higher than that in Hongkong (1.2±0.4%) (Xu et al., 2015), Beijing (1.3%) (Zhang et al., 2018a) and Jinan (0.53±0.20%) (Li et al., 2018) using the same method, while is comparable with the result measured in tunnel experiments (2.1%) carried out in Beijing (Yang et al., 2014). Secondly, low HONO concentration should be companied with high NO_x and high ratio of $\Delta NO/\Delta NO_x$ if direct emission from vehicles was the major source of HONO and the source from secondary formation was negligible in the

394 urban atmosphere. Therefore, we further estimated the HONO/NO_x ratio using a low
395 limit correlation method (Li et al., 2012). In the 2D space of HONO verse NO_x (Fig.
396 S8), the lowest marge with ΔNO/ΔNOx larger than 0.8 were chosen for linear
397 correlation. The ratio of ΔHONO/ΔNOx is 1.17±0.05%. It should be pointed out that
398 the interference from the sampling inlet overestimated 6.7 % of HONO concentration
399 based on control experiments with 100 ppb of NO_2 at 50 % RH. Thus, the ratio of
400 ΔHONO/ΔNOx should be 1.09±0.05% when the interference from the sampling inlet
401 was taken into consideration. This value is lower than that estimated through empirical
402 method discussed above, while is very close to that measured in Hongkong (1.2±0.4%)
403 (Xu et al., 2015) and (1.23±0.35%) (Liang et al., 2017), Guangzhou (1.0%) (Li et al.,
404 2012) and Beijing (1.3% and 1.41 %) (Zhang et al., 2018a;Meng et al., 2019). Finally,
405 several studies have measured the direct emission of HONO from vehicle exhaust. The
406 HONO/NO_x was 0.18% from gasoline cars through chassis dynamometer tests in China
407 (Liu et al., 2017d), while it was 0-0.95% for gasoline vehicles and 0.16-1.0 % for diesel
408 vehicles measured under real-world driving test cycles in Japan (Trinh et al., 2017).
409 Thus, three levels of vehicle emission factor were considered. 1.09±0.05% was taken
410 as the middle value which is very close to the mean emission ratio (1.21) for all of these
411 reported values in China (Li et al., 2018;Xu et al., 2015;Yang et al., 2014;Liu et al.,
412 2017d;Gall et al., 2016;Meng et al., 2019), while 0.18% (Liu et al., 2017d) and 1.8 %
413 were the lower limit and the upper limit, respectively.

414 The $E_{vehicle}$ was calculated using the hourly NO_x emission inventory from vehicles
415 in Beijing (Yang et al., 2019) after converted to emission flux of HONO ($F_{HONO}=F_{NOx}\times$

HONO/NO_x) and the PBL height as described in Section 2.2. Thus, the calculated emission rate reflected the diurnal variation of both the emission inventory and the PBL height. The calculated hourly middle value of $E_{vehicle}$ using the HONO/NO_x of 1.09% was from 0.079±0.038 to 0.32±0.15 ppbv h^{-1}, which was slightly higher than the daytime emission rate of HONO in Xi'an (Huang et al., 2017b). This is reasonable when the vehicle population in Beijing is taken into consideration. The lower limit of $E_{vehicle}$ was 0.013±0.006-0.053±0.023 ppbv h^{-1}, which was close to the estimated emission rate of HONO in Jinan (Li et al., 2018). The upper limit was in the range of 0.13±0.06-0.53±0.23 ppbv h^{-1}.

Soil emission. The emission flux of HONO from soil depends on the water content, the nitrogen nutrient content and the temperature of soil (Oswald et al., 2013). Oswald et al. (2013) measured the emission flux of HONO from 17 soil samples, including eucalyptus forest, tropical rain forest, coniferous forest, pasture, woody savannah, grassland, stone desert, maize field, wheat field, jujube field and cotton field etc. Tropical rain forest, coniferous forest and grassland are the typical plants in downtown Beijing (Huang et al., 2017a). At the same time, their emission fluxes of HONO are comparable (Oswald et al., 2013). Thus, we used the emission flux from grassland to calculate the emission rate of HONO from soil in Beijing because the temperature and water holding content dependent emission flux of HONO from grassland soil was available. Three levels of water content including 25-35%, 35-45% and 45-55% were considered. The temperature dependence of F_{HONO} was calculated using the mean value of the F_{HONO} with different water content, while the low limit and upper limit of F_{HONO}

were calculated using the emission flux from 45-55% of water content and 25-35% of water content, respectively. The lower limit, the middle value and the upper limit of the E_{soil} are 0.0032±0.0027-0.013±0.014, 0.0046±0.0039-0.020±0.20 and 0.0057±0.0047-0.025±0.024 ppbv h^{-1}, respectively, calculated according to Eq. (2).

Homogeneous reaction between NO and OH. Direct measurement of OH concentration was unavailable in this work, while several methods were used to estimate the ambient OH concentration. In winter in Beijing, it has been found that the OH concentration is linearly correlated with J_{O1D}, that's, $c_{OH}=J_{O1D}\times2\times10^{11}$ molecules cm^{-3} (Tan et al., 2019). However, Tan et al. (2018) reported a larger conversion factor (4.33×10^{11} molecules cm^{-3}). Li et al. (2018) estimated the OH radical concentration considering both photolysis rate and NO_2 concentration, namely,

$$c_{OH} = \frac{4.1\times10^{9}\times(J_{O1D})^{0.83}\times(J_{NO_2})^{0.19}\times(140c_{NO_2}+1)}{0.41c_{NO_2}^{2}+1.7c_{NO_2}+1} \quad (15)$$

Overall, the estimated OH concentrations according to Eq. (15) were comparable with that estimated by Tan et al. (2019) (Fig. S10C). The method for the photolysis rates calculation were shown in SI and the time series of the photolysis rates were shown in Fig. S7. On polluted days, high concentration of NO_2 resulted into lower OH concentrations estimated using the Eq. (15). Therefore, the corresponding $P_{NO\text{-}OH}$ was taken as the low limit for homogeneous reaction between NO and HONO because polluted events were discussed in this work, while $P_{NO\text{-}OH}$ calculated using the OH concentration ($J_{O1D}\times4.33\times10^{11}$ molecules cm^{-3}) (Tan et al., 2018) was taken as the upper limit and $P_{NO\text{-}OH}$ calculated using the OH concentration ($J_{O1D}\times2\times10^{11}$ molecules cm^{-3}) (Tan et al., 2019) was the middle value. In the night, OH concentration usually varied

460 from 1.0×10^5 molecules cm^{-3} (Li et al., 2012;Tan et al., 2018) in winter to 5×10^5

461 molecules cm^{-3} in summer (Tan et al., 2017). The nighttime OH concentration was

462 estimated linearly correlated with the product of nighttime O_3 concentration and alkenes

463 concentration, namely,

464 $$c_{OH,night} = 1\times10^5 + 4\times10^5 \times \frac{(c_{O_3}\times c_{alkenes})_{night} - (c_{O_3}\times c_{alkenes})_{night,min}}{(c_{O_3}\times c_{alkenes})_{night,max} - (c_{O_3}\times c_{alkenes})_{night,min}} \quad (16)$$

465 The time series of OH concentration calculated using different methods was shown in

466 Fig. S11. Thus, the lower limit, the middle value and the upper limit of $P_{NO\text{-}OH}$ were

467 0.007±0.019-0.43±0.26, 0.026±0.053-0.99±0.79 and 0.028±0.053-2.14±1.71 ppbv h^{-1},

468 respectively, calculated according to Eqs. (3) and (4). The calculated middle value of

469 $P_{NO\text{-}OH}$ (with mean daytime value of 0.49±0.35 ppb h^{-1}) was comparable with these

470 estimated values by Li et al. (2018) (0.4 ppb h^{-1}) and Huang et al. (2017b) (0.28 ppb h^{-1}

471). It should be noted that measured NO concentration was used to calculate the $P_{NO\text{-}OH}$.

472 Besides vehicle emission, power plant and industries also contribute NO emission. 40 %

473 of NOx was from vehicle emission according to the emission inventory of NO_x in

474 Beijing (He et al., 2002).

475 It should be noted that OH concentration was estimated based on J_{O1D} (Tan et al.,

476 2019;Tan et al., 2018) or J_{O1D} and J_{NO2} (Li et al., 2018). As discussed in Section 3.2,

477 HONO was an important primary OH source in the daytime. Unfortunately, it could not

478 be parameterized for calculating OH concentration because the measured or modelled

479 OH concentration was unavailable in this work. This might underestimate the early

480 daytime OH concentration, subsequently, the contribution of homogeneous reaction of

481 NO with OH to HONO source. This needs to be further investigated in the future.

Photolysis of nitrate. A recent work reported the photolysis rate of nitrate ($J_{nitrate}$) in ambient $PM_{2.5}$ at a solar zenith angle of 0° (Bao et al., 2018). The $J_{nitrate}$ varied from 1.22×10^{-5} to 4.84×10^{-4} s^{-1} with the mean value of 8.24×10^{-5} s^{-1}. These values were further normalized according to the zenith angle and UV light at our observation station to calculate the low limit, the upper limit and the middle $J_{nitrate}$. The time series of the measured nitrate concentration and the middle value of $J_{nitrate}$ were shown in Fig. 1 and Fig. S7, respectively. Therefore, the corresponding daytime lower limit, the middle value and the upper limit of HONO from photolysis of nitrate were 0.0011±0.0021-0.096±0.092, 0.0072±0.0021-0.66±0.092 and 0.042±0.082-3.86±0.008 ppbv h^{-1}, respectively, calculated in the light of Eqs. (3) and (8).

Heterogeneous reactions of NO_2 on aerosol and ground surface. The production of HONO from heterogeneous reactions of NO_2 on aerosol surface was calculated according to Eqs. (3) and (5). The aerosol surface concentration was measured with a SMPS. The uptake coefficient (γ) of NO_2 on different particles varied from 5×10^{-9} to 9.6×10^{-6} (Ndour et al., 2009;Underwood et al., 2001;Underwood et al., 1999), while it was recommended to be 1.2×10^{-8} (Crowley et al., 2010), which was used to calculate the $P_{aerosol}$ as the base case. It has been found that the γ highly depends on the relative humidity (RH). The low limit bound of $P_{aerosol}$ was calculated based on the RH dependent uptake coefficient of NO_2 on kaolinite ($\gamma_{NO2}=4.47\times10^{39}/(1.75\times10^{46}+1.93\times10^{45}RH)$, while the upper limit of $P_{aerosol}$ was calculated according to the RH dependent γ on hematite ($\gamma_{NO2}=4.46\times10^{39}/(6.73\times10^{44}+3.48\times10^{44}\,RH)$ (Liu et al., 2015). Heterogeneous reaction of NO_2 on black carbon (BC) was also considered in the

night. The surface area concentration of BC was calculated according to its specific area (87 m^2 g^{-1}) (Su et al., 2018) and the measured mass concentration. The γ_{NO2} on BC is 1.17×10^{-5}, with a HONO yield of 0.8 (Han et al., 2013). The light enhanced uptake γ of NO_2 (1.9×10^{-6}) on mineral dust was further parameterized (Ndour et al., 2008) after normalized to the solar radiation intensity in Beijing.

The contribution of heterogeneous reaction of NO_2 on ground surface was calculated similar to that on mineral dust. The same kinetics for heterogeneous reaction of NO_2 on aerosol surface were used to calculate the nighttime contribution of ground surface (Zhang et al., 2016;Aumont et al., 2003). A recent work observed a significant enhancement of NO_2 and HONO formation by UV light on the real urban grime (Liu et al., 2019a). Thus, RH dependent kinetic data measured on urban grime ($\gamma_{NO2}=7.4\times 10^{-7}+5.5\times10^{-8}$ RH) was used to calculate the daytime upper limit for heterogeneous uptake of NO_2 on the ground surface. The A_s of aerosols varied from 1×10^{-4} to 4.8×10^{-3} m^{-1} with a mean value of $1.4\pm0.5\times10^{-3}$ m^{-1} during pollution events. This value is comparable with that used in modeling studies (Zhang et al., 2016;Aumont et al., 2003). The A_s of ground surface which was calculated according to Eq. (6) and (7) varied from 1.5×10^{-3} to 3.85×10^{-2} m^{-1} with a mean value of $1.3\pm0.9\times10^{-2}$ m^{-1} during pollution events. The surface roughness was 3.85 calculated according to Eq. (7). The Y_{HONO} was set to 0.5 because of the hydrolysis reaction of NO_2 (Liu et al., 2015), while it was 0.8 for light enhanced reaction (Liu et al., 2019a;Ndour et al., 2008) and on BC (Han et al., 2013).

The lower limit, the middle value and the upper limit of $P_{aerosol}$ were

526 0.00012±0.00009-0.0025±0.0021, 0.00043±0.00020-0.0028±0.0038 and
527 0.0022±0.0012 - 0.0050±0.0038 ppbv h^{-1}, respectively. The corresponding values were
528 0.00027±0.00017-0.0020±0.0012, 0.0014±0.00095-0.0089±0.006 and 0.0025±0.0023-
529 0.060±0.032 ppbv h^{-1} for P_{ground}. The $P_{aerosol}$ calculated in this work was much lower
530 than that estimated by Huang et al. (Huang et al., 2017b) because different calculation
531 methods have been used. In their work, the production rate of HONO was estimated
532 based on the conversion rate (Huang et al., 2017b), whilst it was calculated based on
533 the measured aerosol surface area concentration and uptake coefficient of NO_2 on
534 different particles in this work. In addition, the calculated $P_{aerosol}$ was 2-4 orders of
535 magnitude lower than other sources due to the very small γ_{NO2} on particle surface.
536 It should be pointed out that HONO production from heterogeneous reaction of
537 NO_2 on both aerosol and ground surface greatly depend on the $\gamma_{NO2,\,BET}$ and A_s. The A_s
538 of aerosols is comparable with the modeling input. However, the small nighttime $\gamma_{NO2,}$
539 $_{BET}$ (10^{-8} - 10^{-7}) were used in this work rather than the $\gamma_{NO2,\,BET}$ (1×10^{-6}) used in
540 modeling studies (Zhang et al., 2016;Aumont et al., 2003;Gall et al., 2016). This leads
541 to a lower production rate of HONO from heterogeneous reaction of NO_2 on aerosols.
542 As for heterogeneous reaction of NO_2 on ground surface, besides the small $\gamma_{NO2,\,BET}$
543 used in this work, the A_s of ground surface (0.0015 to 0.0385 m^{-1}), which was calculated
544 using the surface roughness and the PBL height, was also significantly lower than the
545 fixed value of 0.3 m^{-1} in modeling studies that might overestimate the contribution of
546 HONO production from heterogeneous reaction of NO_2 on ground surface. It should be
547 noted that the initial uptake coefficient (γ_{ini}) was parameterized in this work. This will

548 overestimate the contribution of heterogeneous reaction of NO_2 to HONO source
549 because the steady-state uptake coefficient is usually one order of magnitude lower than
550 γ_{ini} (Han et al., 2013;Liu et al., 2015). These results mean that heterogeneous reaction
551 should be unimportant for HONO source in Beijing.

552 **Sinks of HONO.** The loss rates of HONO by photolysis ($L_{photolysis}$), homogeneous
553 reaction with OH radicals ($L_{HONO-OH}$) and dry deposition were calculated according to
554 Eqs. (9)-(11). The daytime J_{HONO} varied from 1.71×10^{-5} to 1.13×10^{-3} s^{-1} on polluted
555 days in winter, while it was in the range of 5.89×10^{-5} to 1.53×10^{-3} s^{-1} from April to June.
556 These values are comparable to modeling results (3.9×10^{-5}-1.8×10^{-3} s^{-1}) (Gall et al.,
557 2016). The daytime $L_{photolysis}$ were in the range of 0.03-5.23 ppb h^{-1} and 0.25-7.10 ppb
558 h^{-1} in winter and the rest months, respectively. It was the major sink of HONO in the
559 daytime. The $L_{HONO-OH}$ varied from 0.0049 to 0.069 ppbv h^{-1} in winter using the $k_{HONO-OH}$
560 of 6×10^{-12} cm^3 $molecule^{-1}$ s^{-1} (Atkinson et al., 2004) and the middle value of OH
561 concentrations. It was from 0.0050 to 0.085 ppbv h^{-1} from April to June. The $L_{deposition}$
562 was in the range of 0.004-0.056 ppbv h^{-1} in winter and 0.004-0.030 ppbv h^{-1} from April
563 to June, calculated according to Eq. (11).

564 As pointed in Section 2.2, vertical transport by advection is an important nocturnal
565 sink of HONO (Gall et al., 2016). In this work, the vertical distribution of HONO
566 concentration is unavailable. Recently, Meng et al. (2019) measured the vertical
567 distribution of HONO in Beijing in December, 2016. The concentration of HONO
568 showed nearly flat profiles from ground level to 240 m in pollution events after sunset,
569 while negative profiles of HONO were observed in pollution events during night (Meng

et al., 2019). The nighttime concentration gradient was 0.0047±0.0025 ppb m^{-1} derived from the nighttime dataset (Meng et al., 2019). Because the daytime vertical gradient of HONO concentration is unavailable in Beijing, we do not calculate the daytime vertical transport. On the other hand, the eddy diffusivity of heat in urban environment was measured in New Delhi, Indian (Yadav et al., 2003). Using their dataset with the wind speed lower than 2.0 m s^{-1}, we derived the relationship between the K_h and the wind speed (WS) (K_h=0.9389×WS-0.3374 m^2 s^{-1}). The nighttime $T_{vertical}$ changed from 0.15 to 0.37 ppbv h^{-1} in winter, while it was from 0.12 to 0.68 ppbv h^{-1} according to Eq. (12) from April to June. Because the wind speed was usually lower than 1.0 m s^{-1} in pollution events (Fig. S6), the contribution of horizontal transport to the daytime HONO sources or sinks decreased because of the short lifetime of HONO. In the night, 79 % of the surface wind speed was lower than 1.0 m s^{-1} on pollution days when the $PM_{2.5}$ concentration was larger than 50 μg m^{-3} and the RH was less than 90 % in winter, thus the air masses from suburban areas should have influence on the sources and sinks of HONO in Beijing. If the HONO concentration at background is zero, the vertical and horizontal transport rate of HONO varied from 0.17 to 0.61 ppbv h^{-1} which is calculated in the light of Eq. (13) on haze days in winter and from 0.15 to 0.74 ppbv h^{-1} in pollution events from April to June. These values are is higher than that calculated according to Eq. (12). Because the background HONO concentration was unavailable, we only considered the nighttime transport calculated according to Eq. (12) in the following section.

Comparison among different HONO sources. Fig. 3 summarizes the diurnal patterns

592 of each sources with different parameterizations during the pollution events from
593 February to March. The black dots and lines mean the middle values, while the shadow
594 indicates the corresponding lower bound and upper bound. In the nighttime, vehicle
595 and soil emission, and homogeneous reaction between NO and OH were the important
596 sources of HONO. In the daytime, however, photolysis of nitrate and homogeneous
597 reaction between NO and OH dominated the sources of HONO. Heterogeneous
598 reactions of NO_2 on aerosol surface and ground surfaces were unimportant compared
599 with other sources because of the very low uptake coefficient compared with modeling
600 studies (Zhang et al., 2016;Aumont et al., 2003).

601 Fig. 4A-F shows the HONO budget estimated using the middle values among these
602 parameters during the polluted events. The mean production rate of HONO varied in
603 the range of 0.16 - 1.76 ppbv h^{-1} from these identified sources, while the corresponding
604 loss rate was from 0.21 to 2.34 ppbv h^{-1} during the polluted events in winter. The main
605 loss of HONO was the photolysis during the daytime (1.74± 0.44 ppbv h^{-1}), whereas it
606 was vertical transport in the nighttime (0.28±0.08 ppbv h^{-1}). Direct emission from
607 vehicles exhaust was the largest nighttime source of HONO (0.22±0.06 ppbv h^{-1}),
608 followed by homogeneous reaction between NO and OH (0.04±0.01 ppbv h^{-1}),
609 emission from soil (0.014±0.005 ppbv h^{-1}), heterogeneous reactions of NO_2 on the
610 ground surface (0.006±0.002 ppbv h^{-1}) and heterogeneous reactions of NO_2 on aerosol
611 surface (0.0005±0.0001 ppbv h^{-1}). $P_{NO\text{-}OH}$ and $P_{nitrate}$ dominated the daytime HONO
612 production, with daytime mean values of 0.49±0.35 ppbv h^{-1} and 0.34±0.23 ppbv h^{-1},
613 respectively. As shown in Fig. 4, these six sources still underestimated the daytime

614 sources of HONO. The $P_{unknown}$ was 0.25±0.24 ppbv h^{-1} in February and March, while
615 it was 0.50±0.38 ppbv h^{-1} from April to June.

616 The $E_{vehicle}$ contributed 57.3±17.9% and 33.9±15.2% to the nighttime HONO
617 sources from February to March and the rest months, respectively, even when the
618 $P_{unknown}$ was taken into consideration. The relative contribution of daytime $E_{vehicle}$
619 decreased to 12.6±14.3% in winter and 9.3±8.4% from April to June. Thus, the daily
620 mean fraction of the $E_{vehicle}$ was 40.5±27.5% and 24.3±17.7% from February to March
621 and from April to June, respectively. This means that the $E_{vehicle}$ dominates the nighttime
622 HONO source during the polluted events in Beijing, which is consistent with the
623 previous result that vehicle emission was the major nighttime HONO source (51.1 % -
624 52 %) in Beijing (Zhang et al., 2019b;Meng et al., 2019). As pointed out in Section 3.3,
625 $E_{vechicle}$ was calculated based on the NO_x inventory from vehicle sector. On the other
626 hand, NO is prone to be quickly converted to NO_2 and NO_z (including HONO, HNO_3,
627 N_2O_5, PAN and organonitrate etc) by O_3, HO_2, RO_2 and OH in the atmosphere. It is
628 reasonable to assume that local traffic emission dominates the ambient NO source in
629 the urban environment. Thus, homogeneous reaction between NO and OH in the
630 atmosphere could also be related to vehicle exhaust. As shown in Fig.3, the diurnal
631 curve of $P_{NO\text{-}OH}$ coincided well with that of OH concentration (Fig. S10). This means
632 the $P_{NO\text{-}OH}$ should be mainly determined by OH concentration. However, the $P_{NO\text{-}OH}$
633 should still reflect the indirect contribution of traffic related emission to HONO source
634 because the ambient NO concentration was used to calculate the $P_{NO\text{-}OH}$. Traffic-related
635 HONO sources ($E_{vehicles}$ +$P_{NO\text{-}OH}$) might contribute 59.3±20.7 % and 36.2±14.4 % to

636 the daily HONO source in winter and the rest months, respectively. Even if 40 % of
637 NO_x was from vehicle exhaust in Beijing (He et al., 2002), traffic-related source
638 ($E_{vehicles}$ + 0.4$P_{NO\text{-}OH}$) might still contribute 48.1±24.3 % in winter and 29.6±16.2 %
639 from April to June to the corresponding daily HONO source. The contribution of traffic-
640 related source was still an important daytime source of HONO (42.3±10.3 % for $E_{vehicles}$
641 +$P_{NO\text{-}OH}$, and 24.4±11.3 % for $E_{vehicles}$ + 0.4$P_{NO\text{-}OH}$) on polluted days in winter.
642 As shown in Fig. 3, uncertainties existed when calculating each HONO source. To
643 further understand the role of traffic emission, we also estimated the lower limit of the
644 traffic-related contribution as follows: 1) the lower limit of $E_{vehicle}$ was obtained by
645 using the lowest reported emission ratio of HONO/NO_x from vehicles (0.18%) (Liu et
646 al., 2017d) rather than 1.09%, which was the empirical value calculated based on the
647 field measurement in Fig. S7; 2) the lower limit for homogeneous reaction between NO
648 and OH radical was calculated according to the method by Li et al. (2018); 3) the upper
649 limit of the emission rate from soil was estimated using the emission flux of HONO
650 with low water content (Oswald et al., 2013); 4) the upper limit of HONO production
651 rate from heterogeneous reaction of NO_2 on the aerosol was calculated using the large
652 RH-dependent uptake coefficient of NO_2 on hematite (Liu et al., 2015) rather the value
653 recommended by Crowley et al. (Crowley et al., 2010); 5) the upper limit for
654 heterogeneous reaction on ground surface was calculated using the RH-dependent
655 kinetic data measured on urban grime (Liu et al., 2019a). As shown in Fig. 5, traffic-
656 related source ($E_{vehicles}$ + $P_{NO\text{-}OH}$) contributed 38.0±15.6 % to the daily HONO sources
657 in winter if all NO was assumed to be dominated by local traffic emission, while it was

31.5±17.5 % when 40 % of NO was considered as local traffic emission (He et al., 2002). Under this circumstance, the daytime $P_{unknown}$ of HONO in winter increased to 1.06±0.36 ppbv h^{-1}, which was corresponding to 63.2±10.1 % of the HONO source. This means these assumptions might underestimate the contribution of the HONO sources. In addition, P_{ground}, $P_{aerosol}$ and $P_{nitrate}$ could be also partially related to traffic emission of NO_x (Lee et al., 2016;Tan et al., 2017). These results mean that the contribution of traffic-related emission might be larger than our estimation in this work. Therefore, our work at least suggests that traffic related emission should be a very important HONO source in winter Beijing although more work is required based on comprehensive modeling studies.

4. Conclusions and atmospheric implications.

In this work, we observed the good correlation between the growth of OA and nitrate mass concentration and the consumed HONO from early morning to noon during the polluted days in winter. This suggests that HONO might promote aerosol mass formation in polluted events in Beijing. This promotion effect could be related to OH production from photolysis of HONO on aerosol formation followed by oxidation process of the corresponding precursors. Our observation supports well the recent modeling studies that HONO may significantly promote secondary aerosol mass formation (Zhang et al., 2019a;Zhang et al., 2019b;Xing et al., 2019;An et al., 2013). Based on budget analysis calculations, traffic-related sources (direction emission and conversion of NO from vehicle emission) should be an important contributor to HONO source during polluted days in winter in Beijing. This means that HONO from the

traffic-related sources might have an important role in aerosol mass formation in the atmosphere.

Vehicle population in China is increasing very quickly (Liu et al., 2017b;Wang et al., 2011). Thus, the negative influences of the vehicle emission on air quality will increase especially in populous metropolitan areas (Yang et al., 2019;Guo et al., 2020), such as Beijing and Shanghai, if targeted pollution control technologies are not applied. It has been estimated that the vehicles emission accounted for over 40% of total urban NO_x emissions in Beijing (He et al., 2002). In the atmosphere, NO_x involves very complicated reaction network, from which finally leads to aerosol mass formation and production of ozone in VOC limited environment. At the same time, reactions of NO_x also leads to some reactive NO_z species (Seinfeld and Pandis, 2006). In particular, HONO is an important precursor of OH, which governs the conversion of primary pollutants to secondary pollutants in the atmosphere. Besides indirect production of HONO from NO, vehicles also directly emit HONO as discussed in this work. Even if the low limit of emission factor was used to calculating the HONO source from the vehicles, the traffic-related emission should still be an important source of HONO in winter Beijing. Therefore, this work implies that mitigation of HONO and NO_x emission from vehicles might be an effective way to reduce secondary aerosol mass formation and can have a positive effect on severe haze events in wintertime Beijing.

It should be pointed out that we only considered O_3 and HONO when discussing the sources of OH. Other sources such as HO_2 (and RO_2) with NO, ozonolysis of alkenes and photolysis of OVOCs might also contribute to OH radicals in the

atmosphere (Tan et al., 2018). In the future it will be vital to comprehensively analyze OH sources and to quantify the role of HONO in secondary aerosol mass formation although photolysis of HONO is the major primary OH source in winter. On the other hand, as discussed in Section 3.3, uncertainties about the HONO budget might originate from the emission factors, OH concentration, and reaction kinetics and so on. The source of HONO from vehicles was calculated based on the emission inventories, which should have a significant bias (Squires et al., 2020). For example, the emission flux of NO_x calculated using the emission inventory from Yang et al. (2019) is as 2.4±0.5 times as the reported emission flux reported by Squires et al. (2020). In addition, the exact height of vertical mixing of HONO was assumed to be the same as the PBL height, this might underestimate the contribution of vehicle, soil and heterogeneous reaction on ground surface. To take the next step, it is required to measure the emission factors from vehicle exhaust under real road conditions in the future. When calculating the OH concentration, the factor between OH concentration and J_{O1D} might vary over locations and seasons due to different NO_x/VOCs ratio (Holland et al., 2003). Direct measurements of OH concentration would be helpful for decreasing the uncertainty of both OH sources and HONO budget analysis. The importance of vehicle emission to HONO source also needs to be further confirmed during special periods such as Chinese New Year when vehicle emission reduces obviously in the future. Finally, it is necessary to quantify the contribution of traffic-related source of HONO on OH production and secondary aerosol formation based on modeling studies in the future.

Data availability. The experimental data are available upon request to the corresponding authors.

Supplement. The supplement related to this article is available online at:

Author information

Author contributions. YL, WW and MK designed the experiments. YL wrote the paper and performed HONO budget analysis. YZ, CL, WW, YC, MG and XW carried out HONO measurement. ZF, FZ, JC, WD and KD did aerosol composition measurements. BC and JK did particle size measurements. YW, BH and YW analyzed meteorological data analysis. CY, FB, JK, TP, HH, MG and MK revised the manuscript.

Acknowledgements:

This research was financially supported by the National Natural Science Foundation of China (41877306), the Ministry of Science and Technology of the People's Republic of China (2019YFC0214701), Academy of Finland via Center of Excellence in Atmospheric Sciences (272041, 316114, and 315203) and European Research Council vShandong Universityia ATM-GTP 266 (742206), the Strategic Priority Research Program of Chinese Academy of Sciences and Beijing University of Chemical Technology.

References:

746 Alicke, B., Geyer, A., Hofzumahaus, A., Holland, F., Konrad, S., Patz, H. W., Schafer, J., Stutz, J., Volz-
747 Thomas, A., and Platt, U.: OH formation by HONO photolysis during the BERLIOZ experiment, Journal of
748 Geophysical Research-Atmospheres, 108, 17, 10.1029/2001jd000579, 2003.
749 An, J., Li, Y., Chen, Y., Li, J., Qu, Y., and Tang, Y.: Enhancements of major aerosol components due to
750 additional HONO sources in the North China Plain and implications for visibility and haze, Adv. Atmos.
751 Sci., 30, 57-66, 10.1007/s00376-012-2016-9, 2013.
752 An, Z., Huang, R.-J., Zhang, R., Tie, X., Li, G., Cao, J., Zhou, W., Shi, Z., Han, Y., Gu, Z., and Ji, Y.: Severe
753 haze in northern China: A synergy of anthropogenic emissions and atmospheric processes, Proc. Natl.
754 Acad. Sci. USA, 116, 8657-8666, 10.1073/pnas.1900125116, 2019.
755 Atkinson, R., and Arey, J.: Atmospheric Degradation of Volatile Organic Compounds, Chem. Rev., 103,
756 4605-4638, doi: 10.1021/cr0206420, 2003.
757 Atkinson, R., Baulch, D. L., Cox, R. A., Crowley, J. N., Hampson, R. F., Hynes, R. G., Jenkin, M. E., Rossi, M.
758 J., and Troe, J.: Evaluated kinetic and photochemical data for atmospheric chemistry: Volume I - gas
759 phase reactions of Ox, HOx, NOx and SOx species, Atmos. Chem. Phys., 4, 1461-1738, 10.5194/acp-4-
760 1461-2004, 2004.
761 Aumont, B., Chervier, F., and Laval, S.: Contribution of HONO sources to the NOx/HOx/O3 chemistry in
762 the polluted boundary layer, Atmos. Environ., 37, 487-498, https://doi.org/10.1016/S1352-
763 2310(02)00920-2, 2003.
764 Bao, F., Li, M., Zhang, Y., Chen, C., and Zhao, J.: Photochemical Aging of Beijing Urban PM2.5: HONO
765 Production, Environ. Sci. Technol., 52, 6309-6316, 10.1021/acs.est.8b00538, 2018.
766 Bianchi, F., Kurtén, T., Riva, M., Mohr, C., Rissanen, M. P., Roldin, P., Berndt, T., Crounse, J. D., Wennberg,
767 P. O., Mentel, T. F., Wildt, J., Junninen, H., Jokinen, T., Kulmala, M., Worsnop, D. R., Thornton, J. A.,
768 Donahue, N., Kjaergaard, H. G., and Ehn, M.: Highly Oxygenated Organic Molecules (HOM) from Gas-
769 Phase Autoxidation Involving Peroxy Radicals: A Key Contributor to Atmospheric Aerosol, Chemical
770 Reviews, 119, 3472-3509, 10.1021/acs.chemrev.8b00395, 2019.
771 Cheng, F., Wang, C., Wang, J., Tang, F., and Xi, X.: Trend analysis of building height and total floor space
772 in Beijing, China using ICESat/GLAS data, International Journal of Remote Sensing,, 32, 8823-8835, 2011.
773 Cheng, Y., Zheng, G., Wei, C., Mu, Q., Zheng, B., Wang, Z., Gao, M., Zhang, Q., He, K., Carmichael, G.,
774 Poschl, U., and Su, H.: Reactive nitrogen chemistry in aerosol water as a source of sulfate during haze
775 events in China, Sci. Adv., 2, 10.1126/sciadv.1601530, 2016.
776 Cho, M.-H., Niles, A., uili Huang, Inglese, J., Austin, C. P., Riss, T., and Xia, M.: A bioluminescent
777 cytotoxicity assay for assessment of membrane integrity using a proteolytic biomarker, Toxicol. In Vitro.,
778 22, 1099-1106, 2008.
779 Crowley, J. N., Ammann, M., Cox, R. A., Hynes, R. G., Jenkin, M. E., Mellouki, A., Rossi, M. J., Troe, J., and
780 Wallington, T. J.: Evaluated kinetic and photochemical data for atmospheric chemistry: Volume V –
781 heterogeneous reactions on solid substrates, Atmos. Chem. Phys., 10, 9059-9223, doi: 10.5194/acp-10-
782 9059-2010, 2010.
783 Cui, L., Li, R., Zhang, Y., Meng, Y., Fu, H., and Chen, J.: An observational study of nitrous acid (HONO) in
784 Shanghai, China: The aerosol impact on HONO formation during the haze episodes, Sci. Total Environ.,
785 630, 1057-1070, 10.1016/j.scitotenv.2018.02.063, 2018.
786 Czader, B. H., Choi, Y., Li, X., Alvarez, S., and Lefer, B.: Impact of updated traffic emissions on HONO
787 mixing ratios simulated for urban site in Houston, Texas, Atmos. Chem. Phys., 15, 1253-1263,
788 10.5194/acp-15-1253-2015, 2015.
789 Dillon, M. B., Lamanna, M. S., Schade, G. W., Goldstein, A. H., and Cohen, R. C.: Chemical evolution of

790 the Sacramento urban plume: Transport and oxidation, J. Geophys. Res.- Atmos., 107, ACH 3-1-ACH 3-
791 15, 10.1029/2001jd000969, 2002.
792 Fu, G. Q., Xu, W. Y., Yang, R. F., Li, J. B., and Zhao, C. S.: The distribution and trends of fog and haze in the
793 North China Plain over the past 30 years, Atmos. Chem. Phys., 14, 11949-11958, 10.5194/acp-14-11949-
794 2014, 2014.
795 Gall, E. T., Griffin, R. J., Steiner, A. L., Dibb, J., Scheuer, E., Gong, L., Rutter, A. P., Cevik, B. K., Kim, S., Lefer,
796 B., and Flynn, J.: Evaluation of nitrous acid sources and sinks in urban outflow, Atmos. Environ., 127,
797 272-282, https://doi.org/10.1016/j.atmosenv.2015.12.044, 2016.
798 Gao, W., Tan, G., Hong, Y., Li, M., Nian, H., Guo, C., Huang, Z., Fu, Z., Dong, J., Xu, X., Cheng, P., and Zhou,
799 Z.: Development of portable single photon ionization time-of-flight mass spectrometer combined with
800 membrane inlet, International Journal of Mass Spectrometry, 334, 8-12,
801 https://doi.org/10.1016/j.ijms.2012.09.003, 2013.
802 Guo, S., Hu, M., Zamora, M. L., Peng, J., Shang, D., Zheng, J., Du, Z., Wu, Z., Shao, M., Zeng, L., Molina,
803 M. J., and Zhang, R.: Elucidating severe urban haze formation in China, Proc. Natl. Acad. Sci. USA, 111,
804 17373-17378, 10.1073/pnas.1419604111, 2014.
805 Guo, S., Hu, M., Peng, J., Wu, Z., Zamora, M. L., Shang, D., Du, Z., Zheng, J., Fang, X., Tang, R., Wu, Y.,
806 Zeng, L., Shuai, S., Zhang, W., Wang, Y., Ji, Y., Li, Y., Zhang, A. L., Wang, W., Zhang, F., Zhao, J., Gong, X.,
807 Wang, C., Molina, M. J., and Zhang, R.: Remarkable nucleation and growth of ultrafine particles from
808 vehicular exhaust, Proc. Natl. Acad. Sci. USA, 117 3427-3432, 10.1073/pnas.1916366117, 2020.
809 Hallquist, M., Wenger, J. C., Baltensperger, U., Rudich, Y., Simpson, D., Claeys, M., Dommen, J., Donahue,
810 N. M., George, C., Goldstein, A. H., Hamilton, J. F., Herrmann, H., Hoffmann, T., Iinuma, Y., Jang, M.,
811 Jenkin, M. E., Jimenez, J. L., Kiendler-Scharr, A., Maenhaut, W., McFiggans, G., Mentel, T. F., Monod, A.,
812 Prévôt, A. S. H., Seinfeld, J. H., Surratt, J. D., Szmigielski, R., and Wildt, J.: The formation, properties and
813 impact of secondary organic aerosol: current and emerging issues, Atmos. Chem. Phys., 9, 5155-5236,
814 10.5194/acp-9-5155-2009, 2009.
815 Han, C., Liu, Y., and He, H.: Role of Organic Carbon in Heterogeneous Reaction of NO2 with Soot, Environ.
816 Sci Technol., 47, 3174-3181, 10.1021/es304468n, 2013.
817 Han, X., Zhang, M. G., Skorokhod, A., and Kou, X. X.: Modeling dry deposition of reactive nitrogen in
818 China with RAMS-CMAQ, Atmos. Environ., 166, 47-61, 10.1016/j.atmosenv.2017.07.015, 2017.
819 He, H., Wang, Y., Ma, Q., Ma, J., Chu, B., Ji, D., Tang, G., Liu, C., Zhang, H., and Hao, J.: Mineral dust and
820 NOx promote the conversion of SO2 to sulfate in heavy pollution days, Sci. Rep., 4, 10.1038/srep04172,
821 2014.
822 He, K., Huo, H., and Zhang, Q.: Urban air pollution in China: current status, characteristics, and progress,
823 Annual Review of Energy Environment 27, 397-431, 2002.
824 He, P. Z., Alexander, B., Geng, L., Chi, X. Y., Fan, S. D., Zhan, H. C., Kang, H., Zheng, G. J., Cheng, Y. F., Su,
825 H., Liu, C., and Xie, Z. Q.: Isotopic constraints on heterogeneous sulfate production in Beijing haze, Atmos.
826 Chem. Phys., 18, 5515-5528, 10.5194/acp-18-5515-2018, 2018.
827 Holland, F., Hofzumahaus, A., Schafer, R., Kraus, A., and Patz, H. W.: Measurements of OH and HO2
828 radical concentrations and photolysis frequencies during BERLIOZ, Journal of Geophysical Research-
829 Atmospheres, 108, 22, 10.1029/2001jd001393, 2003.
830 Hou, S., Tong, S., Ge, M., and An, J.: Comparison of atmospheric nitrous acid during severe haze and
831 clean periods in Beijing, China, Atmos. Environ., 124, 199-206,
832 https://doi.org/10.1016/j.atmosenv.2015.06.023, 2016.
833 Huang, H., Chen, Y., Clinton, N., Wang, J., Wang, X., Liu, C., Gong, P., Yang, J., Bai, Y., Zheng, Y., and Zhu,

Z.: Mapping major land cover dynamics in Beijing using all Landsat images in Google Earth Engine, Remote Sensing of Environment, 202, 166-176, https://doi.org/10.1016/j.rse.2017.02.021, 2017a.

Huang, L., Zhao, Y., Li, H., and Chen, Z.: Kinetics of Heterogeneous Reaction of Sulfur Dioxide on Authentic Mineral Dust: Effects of Relative Humidity and Hydrogen Peroxide, Environ. Sci. Technol., 49, 10797-10805, 10.1021/acs.est.5b03930, 2015.

Huang, R.-J., Zhang, Y., Bozzetti, C., Ho, K.-F., Cao, J.-J., Han, Y., Daellenbach, K. R., Slowik, J. G., Platt, S. M., Canonaco, F., Zotter, P., Wolf, R., Pieber, S. M., Bruns, E. A., Crippa, M., Ciarelli, G., Piazzalunga, A., Schwikowski, M., Abbaszade, G., Schnelle-Kreis, J., Zimmermann, R., An, Z., Szidat, S., Baltensperger, U., Haddad, I. E., and Prevot, A. S. H.: High secondary aerosol contribution to particulate pollution during haze events in China, Nature, 514(7521), 218-222, 10.1038/nature13774, 2014.

Huang, R.-J., Yang, L., Cao, J., Wang, Q., Tie, X., Ho, K.-F., Shen, Z., Zhang, R., Li, G., Zhu, C., Zhang, N., Dai, W., Zhou, J., Liu, S., Chen, Y., Chen, J., and O'Dowd, C. D.: Concentration and sources of atmospheric nitrous acid (HONO) at an urban site in Western China, Sci. Total Environ., 593, 165-172, 10.1016/j.scitotenv.2017.02.166, 2017b.

Kanaya, Y., Cao, R., Akimoto, H., Fukuda, M., Komazaki, Y., Yokouchi, Y., Koike, M., Tanimoto, H., Takegawa, N., and Kondo, a. Y.: Urban photochemistry in central Tokyo: 1. Observed and modeled OH and HO2 radical concentrations during the winter and summer of 2004, J. Geophy. Res.- Atmos., 112, 10.1029/2007JD008670, 2007.

Kim, S., VandenBoer, T. C., Young, C. J., Riedel, T. P., Thornton, J. A., Swarthout, B., Sive, B., Lerner, B., Gilman, J. B., Warneke, C., Roberts, J. M., Guenther, A., Wagner, N. L., Dubé, W. P., Williams, E., and Brown, S. S.: The primary and recycling sources of OH during the NACHTT-2011 campaign: HONO as an important OH primary source in the wintertime, J. Geophys. Res.- Atmos., 119, 6886-6896, doi:10.1002/2013JD019784, 2014.

Kroll, J. H., and Seinfeld, J. H.: Chemistry of secondary organic aerosol: Formation and evolution of low-volatility organics in the atmosphere, Atmos. Environ., 42, 3593-3624, 2008.

Kulmala, M.: Build a global Earth observatory, Nature, 553, 21-23, 10.1038/d41586-017-08967-y, 2018.

Lang, J., Zhang, Y., Zhou, Y., Cheng, S., Chen, D., Guo, X., Chen, S., Li, X., Xing, X., and Wang, H.: Trends of PM2.5 and Chemical Composition in Beijing, 2000-2015, Aerosol Air Qual. Res., 17, 412-425, 10.4209/aaqr.2016.07.0307, 2017.

Lee, J. D., Whalley, L. K., Heard, D. E., Stone, D., Dunmore, R. E., Hamilton, J. F., Young, D. E., Allan, J. D., Laufs, S., and Kleffmann, J.: Detailed budget analysis of HONO in central London reveals a missing daytime source, Atmos. Chem. Phys., 16, 2747-2764, 10.5194/acp-16-2747-2016, 2016.

Lelieveld, J., Evans, J. S., Fnais, M., Giannadaki, D., and Pozzer, A.: The contribution of outdoor air pollution sources to premature mortality on a global scale, Nature, 525, 367-371, 10.1038/nature15371, 2015.

Li, D., Xue, L., Wen, L., Wang, X., Chen, T., Mellouki, A., Chen, J., and Wang, W.: Characteristics and sources of nitrous acid in an urban atmosphere of northern China: Results from 1-yr continuous observations, Atmos. Environ., 182, 296-306, https://doi.org/10.1016/j.atmosenv.2018.03.033, 2018.

Li, X., Brauers, T., H¨aseler, R., Bohn, B., Fuchs, H., Hofzumahaus, A., Holland, F., Lou, S., Lu, K. D., Rohrer, F., Hu, M., Zeng, L. M., Zhang, Y. H., Garland, R. M., Su, H., Nowak, A., Wiedensohler, A., Takegawa, N., Shao, M., and Wahner, A.: Exploring the atmospheric chemistry of nitrous acid (HONO) at a rural site in Southern China, Atmos. Chem. Phys., 12, 1497-1513, 2012.

Li, Z. Q., Guo, J. P., Ding, A. J., Liao, H., Liu, J. J., Sun, Y. L., Wang, T. J., Xue, H. W., Zhang, H. S., and Zhu, B.: Aerosol and boundary-layer interactions and impact on air quality, Natl. Sci. Rev., 4, 810-833,

10.1093/nsr/nwx117, 2017.
Liang, Y., Zha, Q., Wang, W., Cui, L., Lui, K. H., Ho, K. F., Wang, Z., Lee, S.-c., and Wang, T.: Revisiting nitrous acid (HONO) emission from on-road vehicles: A tunnel study with a mixed fleet, J. Air Waste Manage. Assoc., 67, 797-805, 10.1080/10962247.2017.1293573, 2017.
Liggio, J., Li, S.-M., Hayden, K., Taha, Y. M., Stroud, C., Darlington, A., Drollette, B. D., Gordon, M., Lee, P., Liu, P., Leithead, A., Moussa, S. G., Wang, D., O'Brien, J., Mittermeier, R. L., Brook, J. R., Lu, G., Staebler, R. M., Han, Y., Tokarek, T. W., Osthoff, H. D., Makar, P. A., Zhang, J., L. Plata, D., and Gentner, D. R.: Oil sands operations as a large source of secondary organic aerosols, Nature, 534, 91-94, 10.1038/nature17646
http://www.nature.com/nature/journal/vaop/ncurrent/abs/nature17646.html#supplementary-information, 2016.
Liu, C., Ma, Z., Mu, Y., Liu, J., Zhang, C., Zhang, Y., Liu, P., and Zhang, H.: The levels, variation characteristics, and sources of atmospheric non-methane hydrocarbon compounds during wintertime in Beijing, China, Atmos. Chem. Phys., 17, 10633-10649, 10.5194/acp-17-10633-2017, 2017a.
Liu, F., Beirle, S., Zhang, Q., van der A, R. J., Zheng, B., Tong, D., and He, K.: NOx emission trends over Chinese cities estimated from OMI observations during 2005 to 2015, Atmos. Chem. Phys., 17, 9261-9275, 10.5194/acp-17-9261-2017, 2017b.
Liu, J., Li, S., Mekic, M., Jiang, H., Zhou, W., Loisel, G., Song, W., Wang, X., and Gligorovski, S.: Photoenhanced Uptake of NO2 and HONO Formation on Real Urban Grime, Environmental Science & Technology Letters, 6, 413-417, 10.1021/acs.estlett.9b00308, 2019a.
Liu, T., Gong, S., He, J., Yu, M., Wang, Q., Li, H., Liu, W., Zhang, J., Li, L., Wang, X., Li, S., Lu, Y., Du, H., Wang, Y., Zhou, C., Liu, H., and Zhao, Q.: Attributions of meteorological and emission factors to the 2015 winter severe haze pollution episodes in China's Jing-Jin-Ji area, Atmos. Chem. Phys., 17, 2971-2980, 10.5194/acp-17-2971-2017, 2017c.
Liu, Y., Han, C., Ma, J., Bao, X., and He, H.: Influence of relative humidity on heterogeneous kinetics of NO2 on kaolin and hematite, Phys. Chem. Chem. Phys., 17, 19424-19431, doi: 10.1039/C5CP02223A, 2015.
Liu, Y., Lu, K., Ma, Y., Yang, X., Zhang, W., Wu, Y., Peng, J., Shuai, S., Hu, M., and Zhang, Y.: Direct emission of nitrous acid (HONO) from gasoline cars in China determined by vehicle chassis dynamometer experiments, Atmos. Environ., 169, 89-96, 10.1016/j.atmosenv.2017.07.019, 2017d.
Liu, Y., Nie, W., Xu, Z., Wang, T., Wang, R., Li, Y., Wang, L., Chi, X., and Ding, A.: Contributions of different sources to nitrous acid (HONO) at the SORPES station in eastern China: results from one-year continuous observation, Atmos. Chem. Phys. Discuss., 2019, 1-47, 10.5194/acp-2019-219, 2019b.
Liu, Y. H., Lu, K. D., Li, X., Dong, H. B., Tan, Z. F., Wang, H. C., Zou, Q., Wu, Y. S., Zeng, L. M., Hu, M., Min, K. E., Kecorius, S., Wiedensohler, A., and Zhang, Y. H.: A Comprehensive Model Test of the HONO Sources Constrained to Field Measurements at Rural North China Plain, Environ. Sci. Technol., 53, 3517-3525, 10.1021/acs.est.8b06367, 2019c.
Meng, F., Qin, M., Tang, K., Duan, J., Fang, W., Liang, S., Ye, K., Xie, P., Sun, Y., Xie, C., Ye, C., Fu, P., Liu, J., and Liu, W.: High resolution vertical distribution and sources of HONO and NO2 in the nocturnal boundary layer in urban Beijing, China, Atmos. Chem. Phys. Discuss., 2019, 1-34, 10.5194/acp-2019-613, 2019.
Meusel, H., Tamm, A., Kuhn, U., Wu, D., Leifke, A. L., Fiedler, S., Ruckteschler, N., Yordanova, P., Lang-Yona, N., Poehlker, M., Lelieveld, J., Hoffmann, T., Poeschl, U., Su, H., Weber, B., and Cheng, Y.: Emission of nitrous acid from soil and biological soil crusts represents an important source of HONO in the remote

atmosphere in Cyprus, Atmos. Chem. Phys., 18, 799-813, 10.5194/acp-18-799-2018, 2018.
Michoud, V., Colomb, A., Borbon, A., Miet, K., Beekmann, M., Camredon, M., Aumont, B., Perrier, S., Zapf, P., Siour, G., Ait-Helal, W., Afif, C., Kukui, A., Furger, M., Dupont, J. C., Haeffelin, M., and Doussin, J. F.: Study of the unknown HONO daytime source at a European suburban site during the MEGAPOLI summer and winter field campaigns, Atmos. Chem. Phys., 14, 2805-2822, 10.5194/acp-14-2805-2014, 2014.
Ndour, M., D'Anna, B., George, C., Ka, O., Balkanski, Y., K., J., S., and K., A., M.,: Photoenhanced uptake of NO2 on mineral dust: Laboratory experiments and model simulations, Geophys. Res. Lett., 35, L05812. doi:05810.01029/02007GL032006, 2008.
Ndour, M., Nicolas, M., D'Anna, B., Ka, O., and George, C.: Photoreactivity of NO2 on mineral dusts originating from different locations of the Sahara desert, Phys. Chem. Chem. Phys., 11, 1312-1319, 2009.
Oswald, R., Behrendt, T., Ermel, M., Wu, D., Su, H., Cheng, Y., Breuninger, C., Moravek, A., Mougin, E., Delon, C., Loubet, B., Pommerening-Röser, A., Sörgel, M., Pöschl, U., Hoffmann, T., Andreae, M. O., Meixner, F. X., and Trebs, I.: HONO Emissions from Soil Bacteria as a Major Source of Atmospheric Reactive Nitrogen, Science, 341, 1233-1235, 10.1126/science.1242266, 2013.
Oswald, R., Ermel, M., Hens, K., Novelli, A., Ouwersloot, H. G., Paasonen, P., Petäjä, T., Sipilä, M., Keronen, P., Bäck, J., Königstedt, R., Hosaynali Beygi, Z., Fischer, H., Bohn, B., Kubistin, D., Harder, H., Martinez, M., Williams, J., Hoffmann, T., Trebs, I., and Sörgel, M.: A comparison of HONO budgets for two measurement heights at a field station within the boreal forest in Finland, Atmos. Chem. Phys., 15, 799-813, 10.5194/acp-15-799-2015, 2015.
Qin, M., Xie, P., Su, H., Gu, J., Peng, F., Li, S., Zeng, L., Liu, J., Liu, W., and Zhang, Y.: An observational study of the HONO-NO2 coupling at an urban site in Guangzhou City, South China, Atmos. Environ., 43, 5731-5742, 10.1016/j.atmosenv.2009.08.017, 2009.
Ren, X., Brune, W. H., Mao, J., Mitchell, M. J., Lesher, R. L., Simpas, J. B., Metcalf, A. R., Schwab, J. J., Cai, C., Li, Y., Demerjian, K. L., Felton, H. D., Boynton, G., Adams, A., Perry, J., He, Y., Zhou, X., and Hou, J.: Behavior of OH and HO2 in the winter atmosphere in New York City, Atmos. Environ., 40, 252-263, https://doi.org/10.1016/j.atmosenv.2005.11.073, 2006.
Rohrer, F., Bohn, B., Brauers, T., Bruning, D., Johnen, F. J., Wahner, A., and Kleffmann, J.: Characterisation of the photolytic HONO-source in the atmosphere simulation chamber SAPHIR, Atmos. Chem. Phys., 5, 2189-2201, 10.5194/acp-5-2189-2005, 2005.
Sangwan, M., and Zhu, L.: Role of Methyl-2-nitrophenol Photolysis as a Potential Source of OH Radicals in the Polluted Atmosphere: Implications from Laboratory Investigation, J. Phys. Chem. A, 122, 1861-1872, 10.1021/acs.jpca.7b11235, 2018.
Seinfeld, J. H., and Pandis, S. N.: Atmospheric chemistry and physics: From air pollution to climate change, Second ed., John Wiley and Sons, New Jersey, 2006.
Soergel, M., Regelin, E., Bozem, H., Diesch, J. M., Drewnick, F., Fischer, H., Harder, H., Held, A., Hosaynali-Beygi, Z., Martinez, M., and Zetzsch, C.: Quantification of the unknown HONO daytime source and its relation to NO2, Atmos. Chem. Phys., 11, 10433-10447, 10.5194/acp-11-10433-2011, 2011.
Spataro, F., Ianniello, A., Esposito, G., Allegrini, I., Zhu, T., and Hu, M.: Occurrence of atmospheric nitrous acid in the urban area of Beijing (China), Sci. Total Environ., 447, 210-224, https://doi.org/10.1016/j.scitotenv.2012.12.065, 2013.
Squires, F. A., Nemitz, E., Langford, B., Wild, O., Drysdale, W. S., Acton, W. J. F., Fu, P., Grimmond, C. S. B., Hamilton, J. F., Hewitt, C. N., Hollaway, M., Kotthaus, S., Lee, J., Metzger, S., Pingintha-Durden, N., Shaw, M., Vaughan, A. R., Wang, X., Wu, R., Zhang, Q., and Zhang, Y.: Measurements of traffic dominated

pollutant emissions in a Chinese megacity, Atmos. Chem. Phys. Discuss., 2020, 1-33, 10.5194/acp-2019-1105, 2020.
Stutz, J., Wong, K. W., and Tsai, C.: Field Observations of Daytime HONO Chemistry and Its Impact on the OH Radical Budget, in: Disposal of Dangerous Chemicals in Urban Areas and Mega Cities, Dordrecht, 2013, 1-14.
Su, H., Cheng, Y. F., Shao, M., Gao, D. F., Yu, Z. Y., Zeng, L. M., Slanina, J., Zhang, Y. H., and Wiedensohler, A.: Nitrous acid (HONO) and its daytime sources at a rural site during the 2004 PRIDE-PRD experiment in China, Journal of Geophysical Research-Atmospheres, 113, 10.1029/2007jd009060, 2008.
Su, P. H., Kuo, D. T. F., Shih, Y. H., and Chen, C. Y.: Sorption of organic compounds to two diesel soot black carbons in water evaluated by liquid chromatography and polyparameter linear solvation energy relationship, Water Res., 144, 709-718, 10.1016/j.watres.2018.07.064, 2018.
Sun, P., Nie, W., Chi, X., Xie, Y., Huang, X., Xu, Z., Qi, X., Xu, Z., Wang, L., Wang, T., Zhang, Q., and Ding, A.: Two years of online measurement of fine particulate nitrate in the western Yangtze River Delta: influences of thermodynamics and N2O5 hydrolysis, Atmos. Chem. Phys., 18, 17177-17190, 10.5194/acp-18-17177-2018, 2018.
Sun, Y. L., Wang, Z. F., Fu, P. Q., Yang, T., Jiang, Q., Dong, H. B., Li, J., and Jia, J. J.: Aerosol composition, sources and processes during wintertime in Beijing, China, Atmos. Chem. Phys., 13, 4577-4592, 10.5194/acp-13-4577-2013, 2013.
Sun, Y. L., Wang, Z. F., Du, W., Zhang, Q., Wang, Q. Q., Fu, P. Q., Pan, X. L., Li, J., Jayne, J., and Worsnop, D. R.: Long-term real-time measurements of aerosol particle composition in Beijing, China: seasonal variations, meteorological effects, and source analysis, Atmos. Chem. Phys., 15, 10149-10165, 10.5194/acp-15-10149-2015, 2015.
Tan, Z., Fuchs, H., Lu, K., Hofzumahaus, A., Bohn, B., Broch, S., Dong, H., Gomm, S., Häseler, R., He, L., Holland, F., Li, X., Liu, Y., Lu, S., Rohrer, F., Shao, M., Wang, B., Wang, M., Wu, Y., Zeng, L., Zhang, Y., Wahner, A., and Zhang, Y.: Radical chemistry at a rural site (Wangdu) in the North China Plain: observation and model calculations of OH, HO2 and RO2 radicals, Atmos. Chem. Phys., 17, 663-690, 10.5194/acp-17-663-2017, 2017.
Tan, Z., Rohrer, F., Lu, K., Ma, X., Bohn, B., Broch, S., Dong, H., Fuchs, H., Gkatzelis, G. I., Hofzumahaus, A., Holland, F., Li, X., Liu, Y., Liu, Y., Novelli, A., Shao, M., Wang, H., Wu, Y., Zeng, L., Hu, M., Kiendler-Scharr, A., Wahner, A., and Zhang, Y.: Wintertime photochemistry in Beijing: observations of ROx radical concentrations in the North China Plain during the BEST-ONE campaign, Atmos. Chem. Phys., 18, 12391-12411, 10.5194/acp-18-12391-2018, 2018.
Tan, Z. F., Lu, K. D., Jiang, M. Q., Su, R., Wang, H. L., Lou, S. R., Fu, Q. Y., Zhai, C. Z., Tan, Q. W., Yue, D. L., Chen, D. H., Wang, Z. S., Xie, S. D., Zeng, L. M., and Zhang, Y. H.: Daytime atmospheric oxidation capacity in four Chinese megacities during the photochemically polluted season: a case study based on box model simulation, Atmos. Chem. Phys., 19, 3493-3513, 10.5194/acp-19-3493-2019, 2019.
Tang, Y., An, J., Wang, F., Li, Y., Qu, Y., Chen, Y., and Lin, J.: Impacts of an unknown daytime HONO source on the mixing ratio and budget of HONO, and hydroxyl, hydroperoxyl, and organic peroxy radicals, in the coastal regions of China, Atmos. Chem. Phys., 15, 9381-9398, 10.5194/acp-15-9381-2015, 2015.
Tian, M., Liu, Y., Yang, F. M., Zhang, L. M., Peng, C., Chen, Y., Shi, G. M., Wang, H. B., Luo, B., Jiang, C. T., Li, B., Takeda, N., and Koizumi, K.: Increasing importance of nitrate formation for heavy aerosol pollution in two megacities in Sichuan Basin, southwest China, Environ. Pollut., 250, 898-905, 10.1016/j.envpol.2019.04.098, 2019.
Tong, S., Hou, S., Zhang, Y., Chu, B., Liu, Y., He, H., Zhao, P., and Ge, M.: Exploring the nitrous acid (HONO)

formation mechanism in winter Beijing: direct emissions and heterogeneous production in urban and suburban areas, Faraday Discuss., 189, 213-230, 10.1039/c5fd00163c, 2016.
Trinh, H. T., Imanishi, K., Morikawa, T., Hagino, H., and Takenaka, N.: Gaseous nitrous acid (HONO) and nitrogen oxides (NOx) emission from gasoline and diesel vehicles under real-world driving test cycles, J. Air Waste Manage. Assoc., 67, 412-420, 10.1080/10962247.2016.1240726, 2017.
Underwood, G. M., Miller, T. M., and Grassian, V. H.: Transmission FT-IR and Knudsen Cell Study of the Heterogeneous Reactivity of Gaseous Nitrogen Dioxide on Mineral Oxide Particles, J. Phys. Chem. A, 103 6184-6190, 1999.
Underwood, G. M., Song, C. H., Phadnis, M., Carmichael, G. R., and Grassian, V. H.: Heterogeneous reactions of NO2 and HNO3 on oxides and mineral dust: A combined laboratory and modeling study, J. Geophy. Res.- Atmos., 106, 18055-18066, 10.1029/2000jd900552, 2001.
Volkamer, R., Sheehy, P., Molina, L. T., and Molina, M. J.: Oxidative capacity of the Mexico City atmosphere – Part 1: A radical source perspective, Atmos. Chem. Phys., 10, 6969-6991, 10.5194/acp-10-6969-2010, 2010.
Vu, T. V., Shi, Z., Cheng, J., Zhang, Q., He, K., Wang, S., and Harrison, R. M.: Assessing the impact of Clean Air Action Plan on Air Quality Trends in Beijing Megacity using a machine learning technique, Atmos. Chem. Phys. Discuss., 2019, 1-18, 10.5194/acp-2019-173, 2019.
Wang, G., Zhang, R., Gomez, M. E., Yang, L., Zamora, M. L., Hu, M., Lin, Y., Peng, J., Guoc, S., Meng, J., Li, J., Cheng, C., Hu, T., Ren, Y., Wang, Y., Gao, J., Cao, J., An, Z., Zhou, W., Li, G., Wang, J., Tian, P., Marrero-Ortiz, W., Secrest, J., Du, Z., Zheng, J., Shang, D., Zeng, L., Shao, M., Wang, W., Huang, Y., Wang, Y., Zhu, Y., Li, Y., Hu, J., Pan, B., Cai, L., Cheng, Y., Ji, Y., Zhang, F., Rosenfeld, D., Liss, P. S., Duce, R. A., Kolb, C. E., and Molina, M. J.: Persistent sulfate formation from London Fog to Chinese haze, Proc. Natl. Acad. Sci. USA, 113, 13630-13635, 2016.
Wang, H., Lu, K., Chen, X., Zhu, Q., Chen, Q., Guo, S., Jiang, M., Li, X., Shang, D., Tan, Z., Wu, Y., Wu, Z., Zou, Q., Zheng, Y., Zeng, L., Zhu, T., Hu, M., and Zhang, Y.: High N2O5 Concentrations Observed in Urban Beijing: Implications of a Large Nitrate Formation Pathway, Environmental Science & Technology Letters, 4, 416-420, 10.1021/acs.estlett.7b00341, 2017a.
Wang, H. C., Lu, K. D., Chen, X. R., Zhu, Q. D., Wu, Z. J., Wu, Y. S., and Sun, K.: Fast particulate nitrate formation via N2O5 uptake aloft in winter in Beijing, Atmos. Chem. Phys., 18, 10483-10495, 10.5194/acp-18-10483-2018, 2018.
Wang, J., Zhang, X., Guo, J., Wang, Z., and Zhang, M.: Observation of nitrous acid (HONO) in Beijing, China: Seasonal variation, nocturnal formation and daytime budget, Sci. Total Environ., 587, 350-359, 10.1016/j.scitotenv.2017.02.159, 2017b.
Wang, S., Nan, J., Shi, C., Fu, Q., Gao, S., Wang, D., Cui, H., Saiz-Lopez, A., and Zhou, B.: Atmospheric ammonia and its impacts on regional air quality over the megacity of Shanghai, China, Sci. Rep., 5, 15842-15842, 10.1038/srep15842, 2015.
Wang, Y. L., Song, W., Yang, W., Sun, X. C., Tong, Y. D., Wang, X. M., Liu, C. Q., Bai, Z. P., and Liu, X. Y.: Influences of Atmospheric Pollution on the Contributions of Major Oxidation Pathways to PM2.5 Nitrate Formation in Beijing, Journal of Geophysical Research-Atmospheres, 124, 4174-4185, 10.1029/2019jd030284, 2019.
Wang, Y. S., Teter, J., and Sperling, D.: China's soaring vehicle population: Even greater than forecasted?, Energy Policy, 39, 3296-3306, 10.1016/j.enpol.2011.03.020, 2011.
Wang, Z., Wang, W., Tham, Y. J., Li, Q., Wang, H., Wen, L., Wang, X., and Wang, T.: Fast heterogeneous N2O5 uptake and ClNO2 production in power plant and industrial plumes observed in the nocturnal

residual layer over the North China Plain, Atmos. Chem. Phys., 17, 12361-12378, 10.5194/acp-17-12361-2017, 2017c.
Wen, L., Xue, L., Wang, X., Xu, C., Chen, T., Yang, L., Wang, T., Zhang, Q., and Wang, W.: Summertime fine particulate nitrate pollution in the North China Plain: increasing trends, formation mechanisms and implications for control policy, Atmos. Chem. Phys., 18, 11261-11275, 10.5194/acp-18-11261-2018, 2018.
Xing, L., Wu, J., Elser, M., Tong, S., Liu, S., Li, X., Liu, L., Cao, J., Zhou, J., El-Haddad, I., Huang, R., Ge, M., Tie, X., Prévôt, A. S. H., and Li, G.: Wintertime secondary organic aerosol formation in Beijing–Tianjin–Hebei (BTH): contributions of HONO sources and heterogeneous reactions, Atmos. Chem. Phys., 19, 2343-2359, 10.5194/acp-19-2343-2019, 2019.
Xu, Z., Wang, T., Wu, J., Xue, L., Chan, J., Zha, Q., Zhou, S., Louie, P. K. K., and Luk, C. W. Y.: Nitrous acid (HONO) in a polluted subtropical atmosphere: Seasonal variability, direct vehicle emissions and heterogeneous production at ground surface, Atmos. Environ., 106, 100-109, 10.1016/j.atmosenv.2015.01.061, 2015.
Yadav, A. K., Raman, S., and Niyogi, D. D. S.: A note on the estimation of eddy diffusivity and dissipation length in low winds over a tropical urban terrain, Pure and Applied Geophysics, 160, 395-404, 10.1007/s00024-003-8785-4, 2003.
Yang, D., Zhang, S., Niu, T., Wang, Y., Xu, H., Zhang, K. M., and Wu, Y.: High-resolution mapping of vehicle emissions of atmospheric pollutants based on large-scale, real-world traffic datasets, Atmos. Chem. Phys., 2019, 8831–8843, 10.5194/acp-2019-32, 2019.
Yang, Q., Su, H., Li, X., Cheng, Y., Lu, K., Cheng, P., Gu, J., Guo, S., Hu, M., Zeng, L., Zhu, T., and Zhang, Y.: Daytime HONO formation in the suburban area of the megacity Beijing, China, Science China-Chemistry, 57, 1032-1042, 10.1007/s11426-013-5044-0, 2014.
Zhang, F., Wang, Y., Peng, J., Chen, L., Sun, Y., Duan, L., Ge, X., Li, Y., Zhao, J., Liu, C., Zhang, X., Zhang, G., Pan, Y., Wang, Y., Zhang, A. L., Ji, Y., Wang, G., Hu, M., Molina, M. J., and Zhang, R.: An unexpected catalyst dominates formation and radiative forcing of regional haze, Proc. Natl. Acad. Sci. USA, 117, 10.1073/pnas.1919343117, 2020.
Zhang, J., An, J., Qu, Y., Liu, X., and Chen, Y.: Impacts of potential HONO sources on the concentrations of oxidants and secondary organic aerosols in the Beijing-Tianjin-Hebei region of China, Sci. Total Environ., 647, 836-852, https://doi.org/10.1016/j.scitotenv.2018.08.030, 2019a.
Zhang, J. M., Yang, L. X., Chen, J. M., Mellouki, A., Jiang, P., Gao, Y., Li, Y. Y., Yang, Y. M., and Wang, W. X.: Influence of fireworks displays on the chemical characteristics of PM2.5 in rural and suburban areas in Central and East China, Sci. Total Environ., 578, 476-484, 10.1016/j.scitotenv.2016.10.212, 2017.
Zhang, J. W., Chen, J. M., Xue, C. Y., Chen, H., Zhang, Q., Liu, X. G., Mu, Y. J., Guo, Y. T., Wang, D. Y., Chen, Y., Li, J. L., Qu, Y., and An, J. L.: Impacts of six potential HONO sources on HOx budgets and SOA formation during a wintertime heavy haze period in the North China Plain, Sci. Total Environ., 681, 110-123, 10.1016/j.scitotenv.2019.05.100, 2019b.
Zhang, L., Wang, T., Zhang, Q., Zheng, J., Xu, Z., and Lv, M.: Potential sources of nitrous acid (HONO) and their impacts on ozone: A WRF-Chem study in a polluted subtropical region, Journal of Geophysical Research-Atmospheres, 121, 3645-3662, 10.1002/2015jd024468, 2016.
Zhang, W., Tong, S., Ge, M., An, J., Shi, Z., Hou, S., Xia, K., Qu, Y., Zhang, H., Chu, B., Sun, Y., and He, H.: Variations and sources of nitrous acid (HONO) during a severe pollution episode in Beijing in winter 2016, The Science of the total environment, 648, 253-262, 10.1016/j.scitotenv.2018.08.133, 2018a.
Zhang, X. Y., Zhong, J. T., Wang, J. Z., Wang, Y. Q., and Liu, Y. J.: The interdecadal worsening of weather

conditions affecting aerosol pollution in the Beijing area in relation to climate warming, Atmos. Chem. Phys., 18, 5991-5999, 10.5194/acp-18-5991-2018, 2018b.
Zheng, B., Zhang, Q., Zhang, Y., He, K. B., Wang, K., Zheng, G. J., Duan, F. K., Ma, Y. L., and Kimoto, T.: Heterogeneous chemistry: a mechanism missing in current models to explain secondary inorganic aerosol formation during the January 2013 haze episode in North China, Atmos. Chem. Phys., 15, 2031-2049, doi: 10.5194/acp-15-2031-2015, 2015a.
Zheng, G. J., Duan, F. K., Su, H., Ma, Y. L., Cheng, Y., Zheng, B., Zhang, Q., Huang, T., Kimoto, T., Chang, D., Pöschl, U., Cheng, Y. F., and He, K. B.: Exploring the severe winter haze in Beijing: the impact of synoptic weather, regional transport and heterogeneous reactions, Atmos. Chem. Phys., 15, 2969-2983, 10.5194/acp-15-2969-2015, 2015b.
Zhu, W. H., Xu, X. D., Zheng, J., Yan, P., Wang, Y. J., and Cai, W. Y.: The characteristics of abnormal wintertime pollution events in the Jing-Jin-Ji region and its relationships with meteorological factors, Sci. Total Environ., 626, 887-898, 10.1016/j.scitotenv.2018.01.083, 2018.
Zou, Y., Deng, X. J., Deng, T., Yin, C. Q., and Li, F.: One-Year Characterization and Reactivity of Isoprene and Its Impact on Surface Ozone Formation at A Suburban Site in Guangzhou, China, Atmosphere, 10, 10.3390/atmos10040201, 2019.

Figure captions

Fig. 1. An overviewed measurement of non-refractory-$PM_{2.5}$ (NR-$PM_{2.5}$), HONO, NOx, $PM_{2.5}$ and meteorological parameters from Feb. 1 to July 1, 2018. (A) the mass concentration of different components of $PM_{2.5}$, (B) the mass fraction of individual component, (C) HONO and NOx concentration, (D) temperature and RH, (E) wind speed and wind direction, (F) UVB and PBL height and (G) visibility and $PM_{2.5}$ concentration during observation. We consider the period before Apr. 1 as winter. During the winter period, 12 cases are selected and numbered, including three clean cases (1, 3, and 5, marked in yellow) and the rest 9 pollution episodes (marked in blue).

Fig. 2. Contribution of HONO to OH production and correlation between OA and HONO concentration. Diurnal production rates of OH from photolysis of HONO and O_3 on polluted days with $PM_{2.5}$ concentration larger than 50 μg m^{-3} and RH less than 90 % (A) from Feb 1 to Mar 31, (B) from Apr 1 to Jun 30; (C) Daytime variation of OA/CO and HONO/CO concentration for the 7^{th} and 12^{th} episodes and (D) correlation of the daytime OA/CO increased and consumed HONO/CO.

Fig. 3. Diurnal pattern of HONO sources calculated with different parameterizations. The low bound, the middle value, and upper bound of (A) soil emission calculated based on 45-55%, 35-45% and 25-35% of water content, (B) vehicle emission with relative emission factor to NOx of 0.18%, 1.17±0.05% and 1.8 %, (C) production from reaction between NO and OH, whose concentration estimated using Xu (Xu et al., 2015), (Tan et al., 2019)

Fig. 4. The budget of HONO (A) and (B) Diurnal production rates of HONO, (C) and

(D) loss rates of HONO, (E) and (F) relative contribution of each source on polluted days with $PM_{2.5}$ concentrations higher than 50 μg m^{-3} and RH less than 90 %. The left column shows the data from February 1 to March 31) and the right one shows the data from April 1 to June 30.

Fig. 5. (A)-(B) Diurnal production rates and (C)-(D) diurnal loss rates of HONO; (E)-(F) relative contribution of HONO sources on polluted days with $PM_{2.5}$ concentrations higher than 50 μg m^{-3} and RH less than 90 %. The $E_{vehicle}$ is calculated using the low limit of HONO/NOx from vehicles (0.18%) (Liu et al., 2017d) and the $P_{NO\text{-}OH}$ is calculated using the low limit of OH concentration, while the upper limit of E_{soil}, $P_{aerosol}$ and P_{ground} are used as described in the text.

Figures

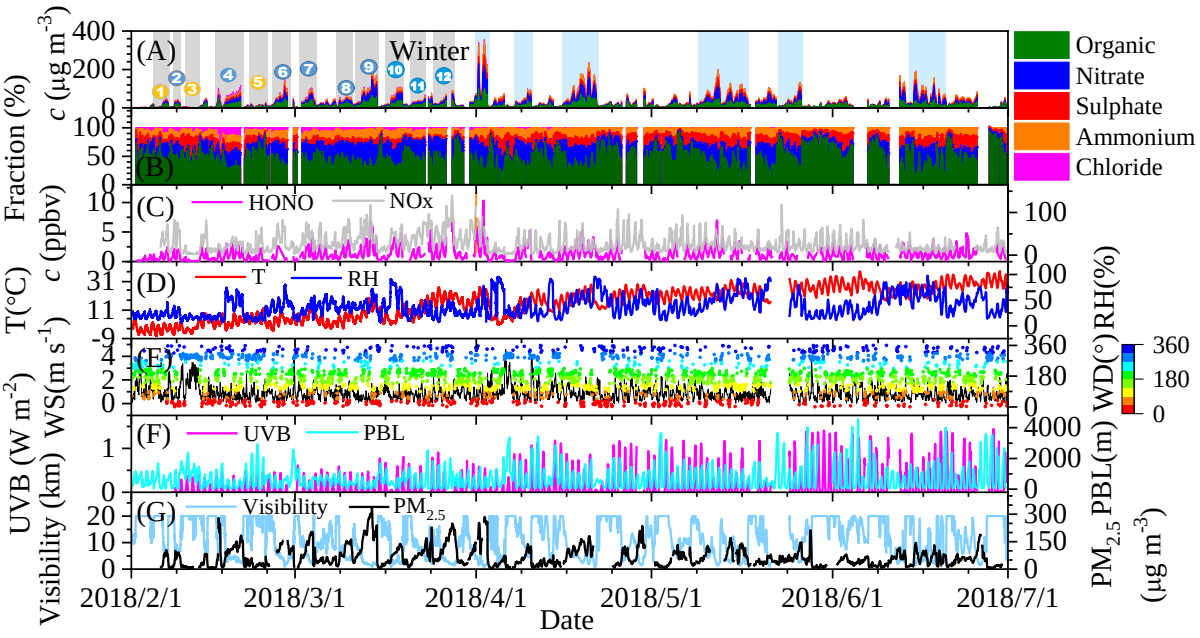

Fig. 1.

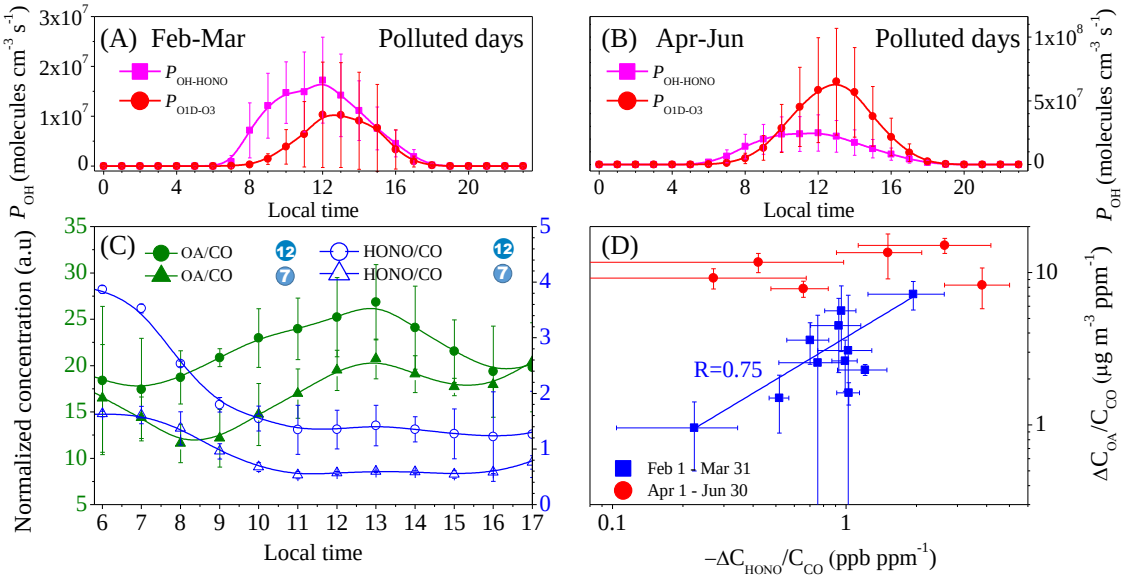
(A) Feb-Mar
Polluted days
$P_{OH-HONO}$
P_{O1D-O3}
Local time
(B) Apr-Jun
Polluted days
P_{OH} (molecules cm^{-3} s^{-1})
(C)
OA/CO
HONO/CO
Normalized concentration (a.u)
Local time
(D)
R=0.75
Feb 1 - Mar 31
Apr 1 - Jun 30
$-\Delta C_{HONO}/C_{CO}$ (ppb ppm^{-1})
$\Delta C_{OA}/C_{CO}$ (μg m^{-3} ppm^{-1})

Fig. 2.

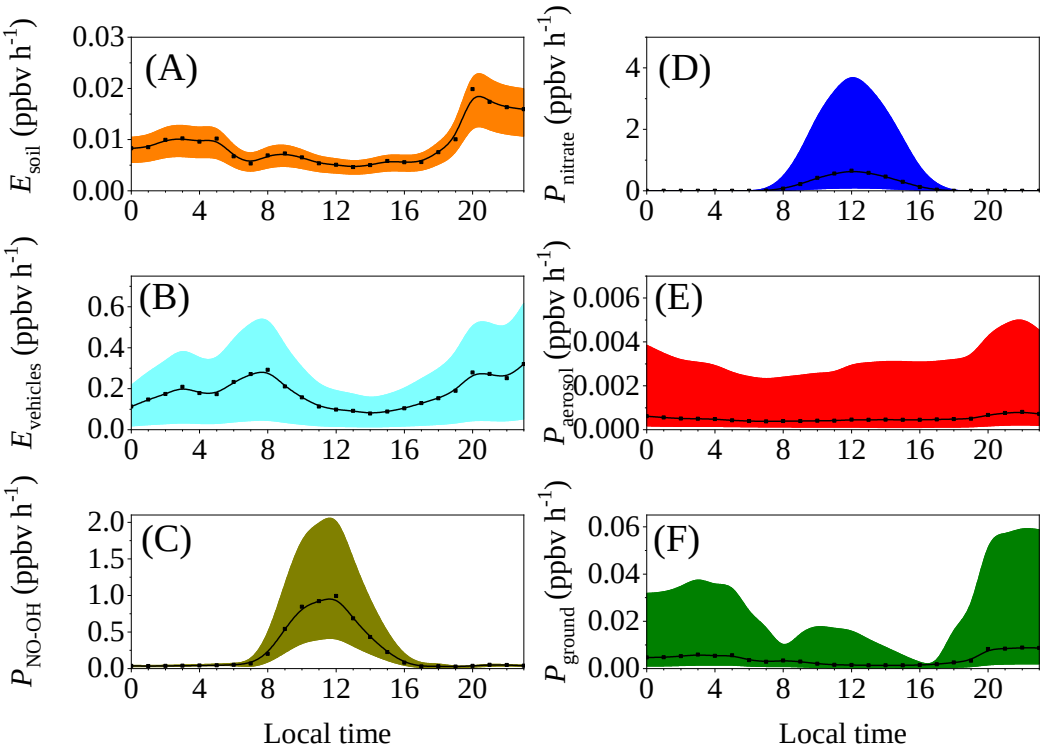
(A)
(B)
(C)
(D)
(E)
(F)
E_{soil} (ppbv h^{-1})
$E_{vehicles}$ (ppbv h^{-1})
P_{NO-OH} (ppbv h^{-1})
$P_{nitrate}$ (ppbv h^{-1})
$P_{aerosol}$ (ppbv h^{-1})
P_{ground} (ppbv h^{-1})
Local time
Local time

Fig. 3

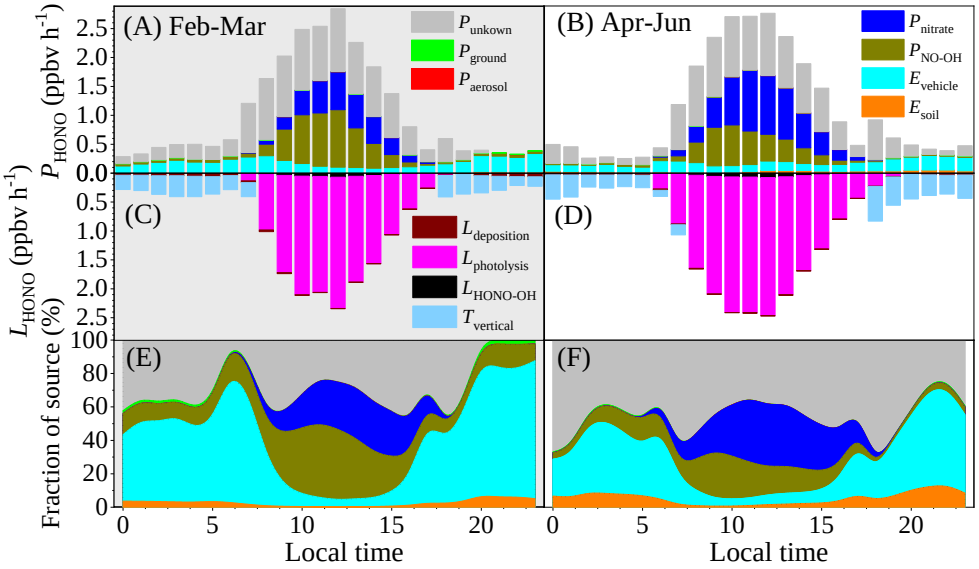

1159

1160

1161 **Fig. 4**.

1162

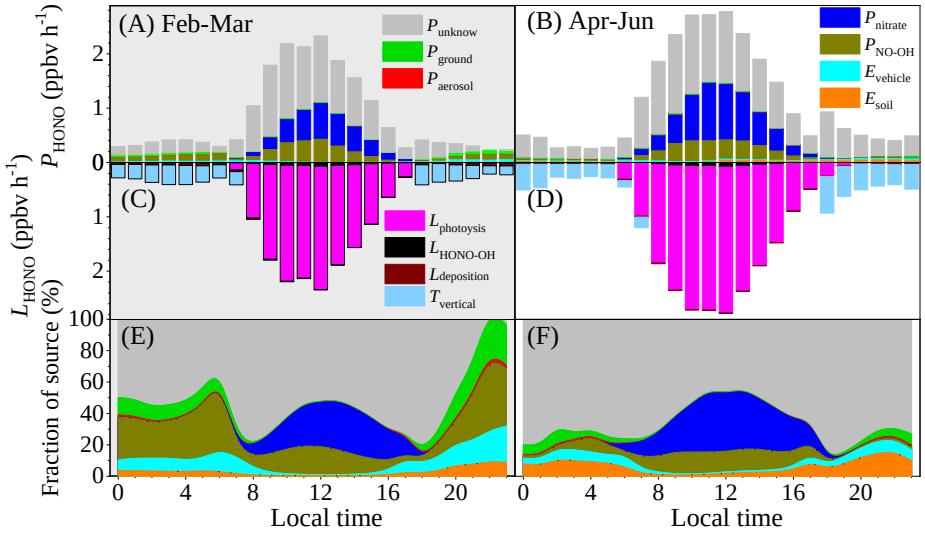

1163

1164 **Fig. 5.**